DESIGN, CONSTRUCTION, and TESTING
of an
ELECTRO-MAGNETICALLY LAUNCHED MODEL GLIDER

by

Marc Jeffrey Zeitlin

B.S. M.I.T.
1979

Submitted in Partial Fulfillment

of the Requirements of the

Degree of

Master of Science

at the

Massachusetts Institute of Technology

August 1981

Signature redacted

Signature of Author. ....
Department of Aero. and Astro. Eng.
August 6, 1981

Signature redacted

Certified by.......................................
Rene Miller
Thesis supervisor

Signature redacted

Accepted by.......................................
Harold Y. Wachman
Chairman, Departmental Graduate Committee

DESIGN, CONSTRUCTION, and TESTING

of an

ELECTRO-MAGNETICALLY LAUNCHED Model GLIDER

by

Marc Jeffrey Zeitlin

Submitted to the Department of Aeronautical Engineering on August 7, 1981 in partial fulfillment of the requirements for the Degree of Master of Science in Aeronautical Engineering

ABSTRACT

A 22 kg. cargo glider for launch from an electromagnetic launcher was desired by the Accelerator group at the National Magnet Laboratory. It was to be accelerated over a three meter length at an average of 100 gees to a velocity of 80 m/sec.

A preliminary study was done by procuring a commercially available model glider, strengthening it, and then doing acceleration tests upon it. This glider withstood 250 gees after modification. It was launched from the electro-magnetic launcher four times, at peak accelerations ranging from 40 gees to 100 gees and peak velocities ranging from 30 m/sec to 45 m/sec.

A half scale cargo glider was designed and constructed. It was built of foam, wood, aluminum tubes and fiberglass-epoxy, and weighed about 4 kg. Flight testing was carried out by conventional launching (Hi-Start) means. Five flights were flown to observe the flight characteristics which were quite satisfactory. The aircraft was stable and docile.

As of this date no electro-magnetic launches have been done with the half scale model, however they are planned for the near future.

II. ACKNOWLEDGEMENTS

As in all research, it has not been possible for me to accomplish what I have without a great deal of help from many people. I would like to thank these people in the Accelerator Group at the Magnet Lab (Peter Mongeau, Fred Williams, Whitney Hamnett, Osa Fitch, and Henry Kolm) for their help in buildiing the gliders and the launching yoke, for their suggestions in design and construction, for the two days they spent dragging the launcher out to Briggs field to test the gliders, and for the time they spent explaining the rudimentary behavior of the high power electrical circuitry and launcher to me. I want to thank Adrian Nye for bringing his expertise and experience in model airplane construction to the group, and for his time and effort in the construction and modification of the gliders. I thank my thesis advisor, Prof. Rene Miller, for always pointing me in the right direction in the design and analysis part of my work, and for knowing what was necessary for me to do next.

Most of all, I wish to thank Jorge Chavier, manager of Family Hobby on Mass. Ave. in North Cambridge, for the many hours he spent talking to me about the project, advising me on design and construction, teaching me to fly radio control models, flight testing the gliders without

and then with the launcher, and being friendly and helpful throughout, taking his one free day a week to help us out.

Without all these people, but especially without Jorge, my task would have been virtually impossible.

TABLE OF CONTENTS

LIST OF SYMBOLS

a - wing lift curve slope (1/rad)

a_1 - horizontal tail lift curve slope (1/rad)

a_2 - elevator lift curve slope (1/rad)

A - moment of inertia about X-axis (kg-m)

b - wing span (m)

B - moment of inertia about Y-axis (kg-m)

c - wing chord (m)

C - moment of inertia about Z-axis (kg-m)

E - product of inertia about Y-axis (kg-m)

E_n - modulus of elasticity (Pa)

F - ultimate strength (Pa)

h - fuselage height (m)

h_o - aerodynamic center position (%c)

h_1 - center of gravity position (%c)

h_n - stick fixed neutral point position (%c)

i_A - non-dimensional moment of inertia (X-axis)

i_B - non-dimensional moment of inertia (Y-axis)

i_C - non-dimensional moment of inertia (Z-axis)

i_E - non-dimensional product of inertia (Y-axis)

I - moment of inertia (m)

K_n - static margin

l - characteristic length

l_H - aerodynamic center distance: wing-vertical tail (m)

l_V - A. C. distance: wing-horizontal tail (m)

L - lift (Nt)

M - moment (Nt-m)

M_g - aircraft mass (kg)

n - load factor

N - cycles to halve

q - dynamic pressure (Nt)

S - wing surface area (m)

S_H - horizontal tail surface area (m)

S_V - vertical tail surface area (m)

t_{half} - halving time (sec)

t - wing thickness (m)

t^* - characteristic time (sec)

T - period (sec)

$\bar{V}'$ - modified tail volume coefficient

V_H - corrected tail volume coefficient

V - velocity (m/sec)

w - fuselage width (m)

w_l - wing lift distribution (Nt/m)

ω - natural frequncy (rad/sec)

W_g - aircraft weight (Nt)

W_w - wing weight (Nt)

X - position in X - direction (m)

Y - position in Y - direction (m)

Z - position in Z - direction (m)

z_w - distance of wing-root quarter chord point below fuselage centerline (m)

z_f - distance of vertical tail aerodynamic center above center of gravity (m)

AR - aspect ratio

S.F. - safety factor

α - angle of attack (rad)

Γ - dihedral angle (deg)

ϵ - downwash induced

$\frac{\partial \epsilon}{\partial \alpha}$ - change in ϵ with α

η - tail incidence angle (rad)

η_T - tail angle with respect to zero lift line (rad)

ρ - density (kg/m)

σ - stress (Pa)

μ - non-dimensional mass

ζ - damping ratio

<u>Aerodynamic</u> <u>Coefficients</u>

C_L - lift

C_m - moment

C_D - drag

C_{LT} - tail lift

C_{L_α} - aircraft lift curve slope

C_{m_α} - change in moment coefficient with angle of attack

C_{X_α} - change in X - direction force with angle of attack

C_{Z_α} - change in Z - direction force with angle of attack

C_{X_u} - change in X - direction force with velocity change

C_{Z_q} - change in lift with pitching velocity

C_{m_q} - change in moment with pitching velocity

$C_{z_{\dot{\alpha}}}$ - change in Z - direction force with rate of angle of attack changes

$C_{m_{\dot{\alpha}}}$ - change in moment with rate of angle of attack changes

C_{y_β} - change in sideforce due to sideslip angle

C_{l_β} - change in rolling moment due to sideslip angle

C_{n_β} - change in yawing moment due to sideslip angle

C_{y_p} - change in Y - direction force with roll rate

C_{n_p} - change in yawing moment due to roll

C_{l_p} - change in rolling moment with roll

C_{y_r} - change in Y - direction force due to yaw rate

C_{l_r} - change in rolling moment due to yaw rate

C_{n_r} - change in yawing moment due to yaw rate

LIST OF TABLES

LIST OF FIGURES

III. INTRODUCTION

A) Motivation

Military resupply of soldiers in mountainous terrain, those only a few miles off, those in need of supplies quickly, or those surrounded by hostile personnel is either a difficult and dangerous task or else one that is time consuming and expensive. For much resupply, helicopters are used to airlift the materials to the soldiers. If they are surrounded by hostile troops, this exposes the multi-million dollar helicopter to anti-aircraft fire. In mountainous terrain, the helicopters have a higher accident rate, so in either of these situations the helicopter is in danger. Helicopters need a crew and support personnel, not to mention refueling and a home base.

A low cost, fast, easy, mobile, low risk system of resupply for these soldiers is needed, especially for those close to the supply point. A system that has been proposed by the Accelerator Group of the Francis Bitter National Magnet Laboratories is to use small remotely piloted or self-guided cargo gliders for the material carrying. These cargo gliders would be launched by an electro-magnetic accelerator being developed by the Accelerator Group. The launcher would be mounted on a truck trailer and powered either by the truck engine or a separate generator.

A cargo glider for this purpose needed to be developed, and this development is the subject of this thesis.

B) Scope

The launcher design has been set by the Accelerator Group, and I will give a short explanation of its design and operation. The launcher is a linear Direct Current Brush Motor, a schematic of which is shown in Figure 1.

FIGURE 1

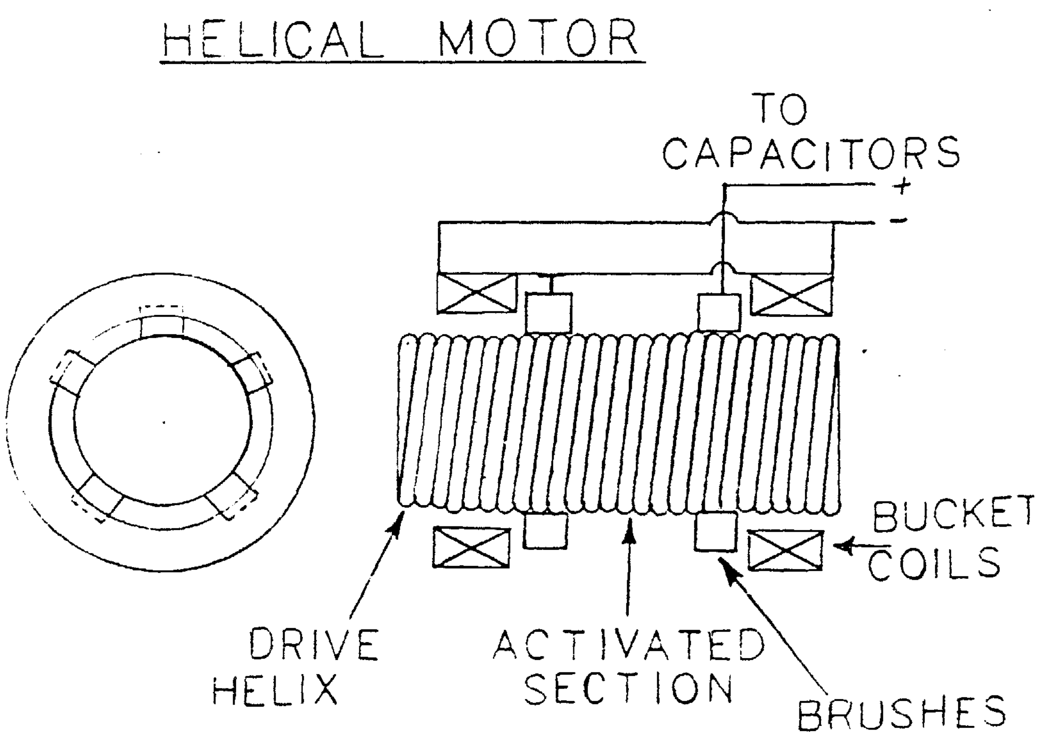

The current passes through the first and second coils in parallel, then through one set of brushes, and into the helix. Exiting the helix through the second set of brushes, it then dumps to ground. This creates a magnetic field associated with each of the coils, and a third field associated with the activated section of the helix. (that between the brush sets). With this arrangement, one coil is attracted to the helix and one is repelled by the helix by the interaction of the coil magnetic fields with the helix magnetic field. This creates a push-pull situation in which the coils and brushes are accelerated and slide along the helix tube. Since the brushes are moving with the coils, the energized section of the helix is always between the coils, keeping the orientation and relation between the magnetic fields the same as the assembly (called the bucket) slides. For as long as current flows there will be a force on the bucket and it will accelerate. If the helix direction on the tube is reversed, the push-pull forces will be reversed and the bucket will decelerate. A bank of capacitors is used to store energy and supply current to the system.

The launcher set up and operation is shown in Figure 2.

FIGURE 2

LAUNCHER SET UP

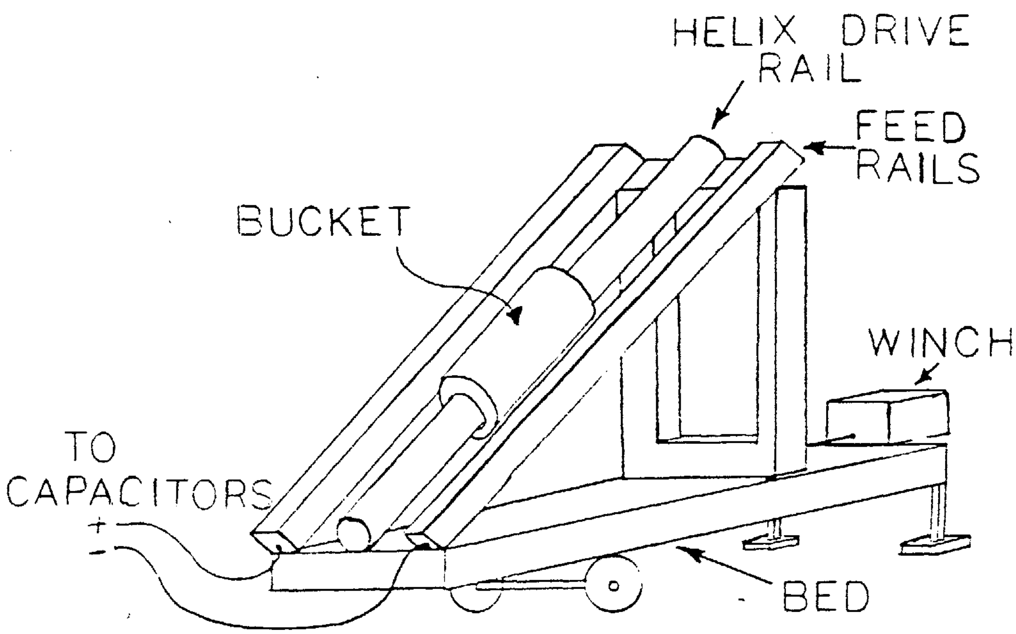

The launcher is mounted on a truck trailer, pulled behind a truck which houses the four 350 volt, one-quarter farad capacitor banks and all the associated electrical equipment. Using a winch and scissors jack arrangement on the trailer, the helix and current feedrails assembly is raised to the launch angle of 45 degrees. The bucket gets current from sliding brushes riding on the feedrails, which are copper strips riveted to four inch square aluminum box beams. The first two thirds of the helix are wound as an acceleration section and the final third as a deceleration section. The acceleration section is three meters long, and the deceleration section is one and a half meters long.

A 22 kg. gross weight cargo glider was envisioned and considered appropriate for the resupply task. A launch velocity of approximately 80 meters per second would be necessary to achieve an eight to sixteen kilometer range with a medium performance glider, and this implies an average acceleration of about 1000 m/sec./sec. (or 100 gee's) over the three meter acceleration length.

I was given the task of developing a glider to meet the demands of a 100 gee, 80 m/sec. launch, along with the associated stability and control criteria. I was also to interface with the launcher crew in the development of the Glider-Launcher Yoke connection.

Three steps were seen as being necessary. The first involved using an existing model glider (probably modified) as a concept test. The second was to design and build a half scale model of the 22 kg. cargo glider and test it. The third was to build a full scale 22 kg. glider. The first two steps have been completed and shall be described in the following chapters.

IV. GLIDER - MARK I

A) Selection

For the concept testing, a commercially available model glider that was easy to build and modify was necessary. To allow for adequate clearance between the glider and the launcher, and provide for the glider-launcher interface, a high wing model was desirable. A stable, easy to fly trainer was preferable, although not necessary. The glider must be able to hold the radio control system used for controlling aircraft maneuvers. A model glider that met these criteria was found and purchased. It was a Model Rectifier Corp. training glider, made of closed cell styrofoam. It was a simple, high wing, radio control glider, shown in Figure 3.

FIGURE 3

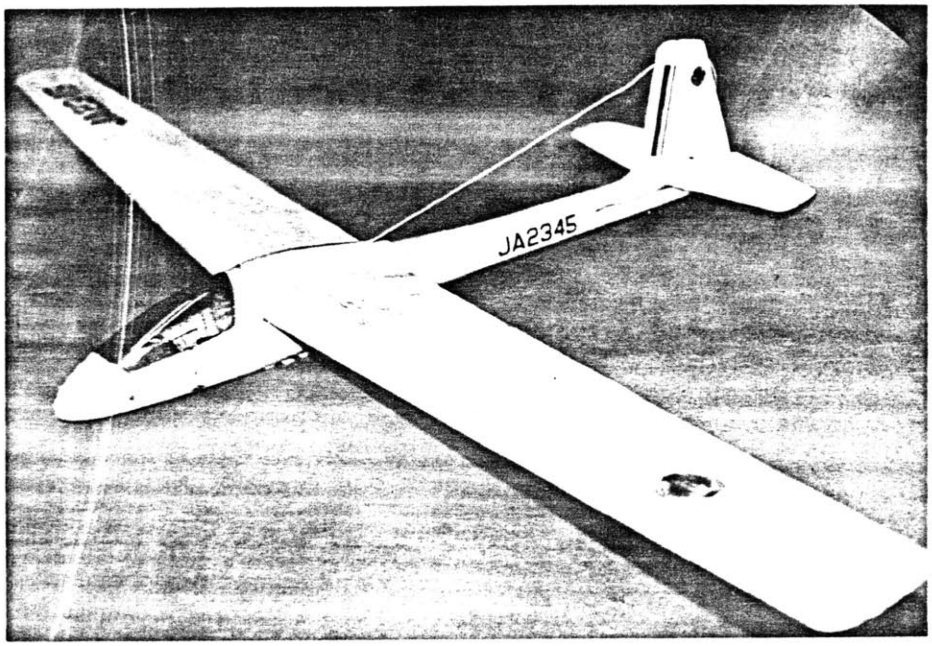

The radio control system needed to be rugged, strong, lightweight, reliable, fast, and available. Kraft has long been the premier radio control manufacturer, and a Kraft 5-channel radio control set was purchased. It had a flying weight of approximately one quarter kilogram. It consisted of a transmitter capable of transmitting commands to independent servo-mechanisms over a three to five mile range, a receiver capable of receiving and decoding the transmissions, three heavy duty electro-mechanical servo-mechanisms, one normal servo, and a nickel-cadmium battery pack to power the receiver and the servos. This system is shown in Figure 4.

FIGURE 4

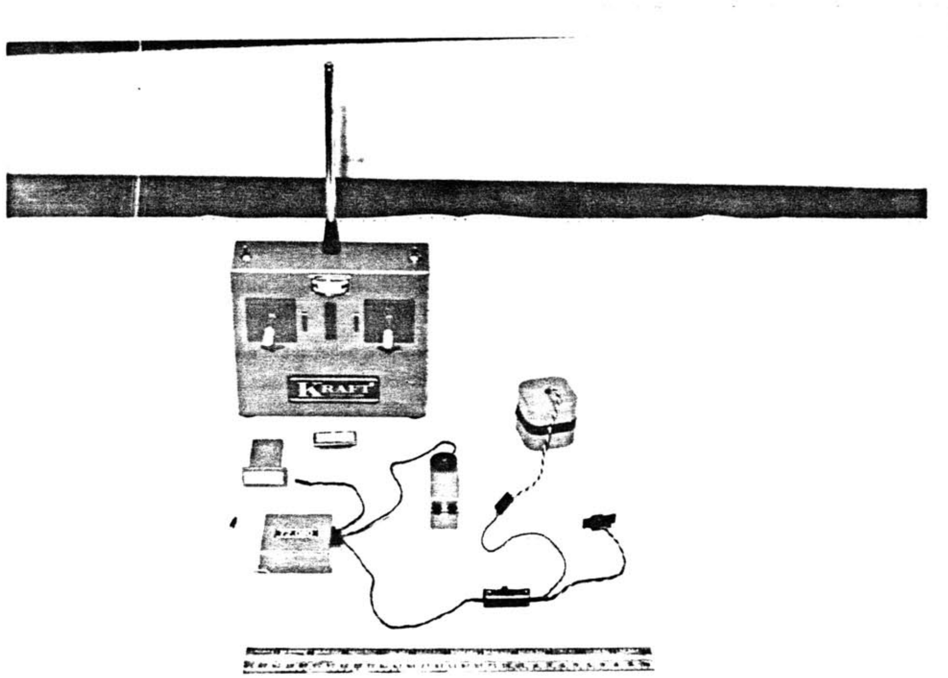

The Mark I glider was smaller than the proposed cargo glider, and also only needed two channels of the radio control set (rudder and elevator control), so a miniature receiver and a pair of subminiature servos were borrowed from Jorge Chavier. These are shown in Figure 5 with a heavy duty servo for size comparison.

FIGURE 5

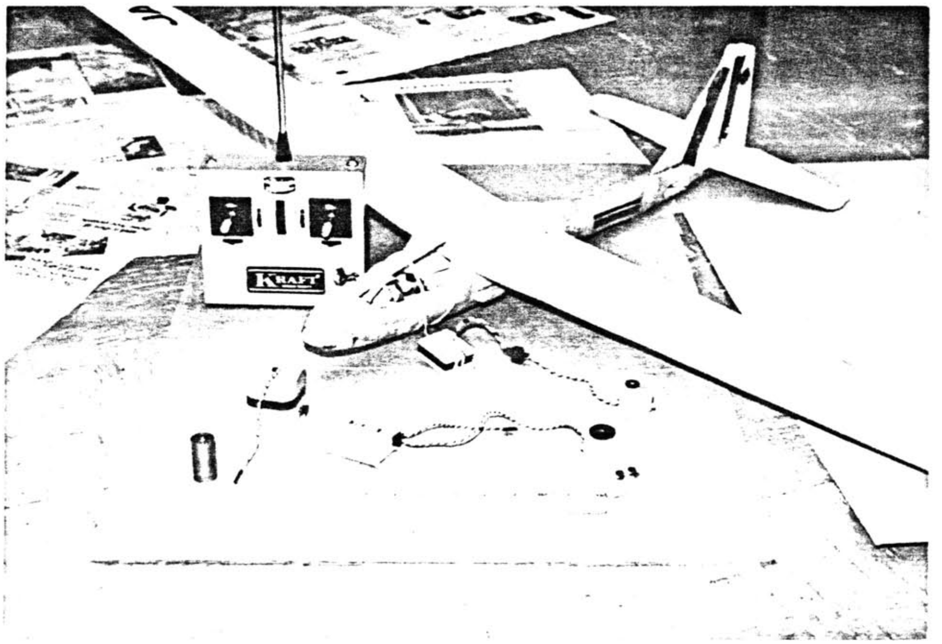

B) Modifications and Yoke Construction

To allow the simple foam glider to withstand the acceleration and speed imposed by the launcher, structural strengthening was necessary. By far the simplest and easiest method of structural reinforcement of the foam glider (and the basic reason a foam glider was chosen) was to use the foam as a core for a fiberglass-epoxy skin. This would not appreciably change the aerodynamic characteristics of the glider, which were known. It would also be useful as practice in methodology, since the wings of the cargo glider were to be fiberglass-epoxy covered foam. The fiberglass-epoxy matrix provides good impact protection of the radio control unit; witness construction of motorcycle helmets.

Fiberglass cloth weighing 6 oz./sq. m. and Hobbypoxy epoxy #2 were used. Each of the airplane parts was coated with a thin layer of epoxy and then a layer of fiberglass cloth, with the weave oriented as in Figure 6, at 45 degrees to the major axis of the part.

FIGURE 6

FIBERGLASS CLOTH
WEAVE ORIENTATION

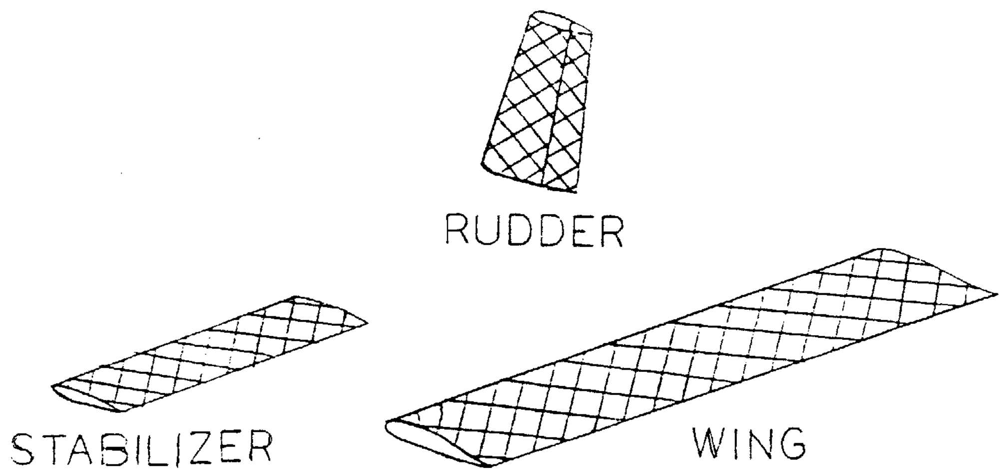

The fiberglass was smoothed down so that the epoxy was forced up through the weave. The wing was given two layers of the cloth, while all other parts had one layer. When the epoxy hardened the glider was assembled and epoxied together. The bottom of the fuselage had another layer of fiberglass added for abrasion protection during landings. Adding the fiberglass-epoxy approximately doubled the weight of the aircraft, from one half to one kilograms. The stock towhook was installed to allow for conventional Hi-Start launches, described later.

The radio control unit was then installed. The battery-pack was installed up inside the nose of the plane, and held in place with a dowel across the fuselage. The receiver was put behind the battery-pack, and restrained in the same manner. The antenna was routed along the side of the fuselage back to the vertical stabilizer, and was held in place with a dab of silicone RTV glue every inch or so. One subminiature servo and the normal duty servo were installed behind the receiver on wooden beams epoxied to the floor of the glider. They were hooked up to the rudder and elevator via the normal pushrods. Because of the distribution of the fiberglass covering, the center of gravity of the aircraft was too far aft, so a brass weight was installed next to the receiver to bring the C.G. to the 30% chord position of the wing, within the normal operating range. The brass weight and the receiver were held down with thin aluminum straps attached to both cross fuselage dowels. The interior of the fuselage is shown in Figure 7.

FIGURE 7

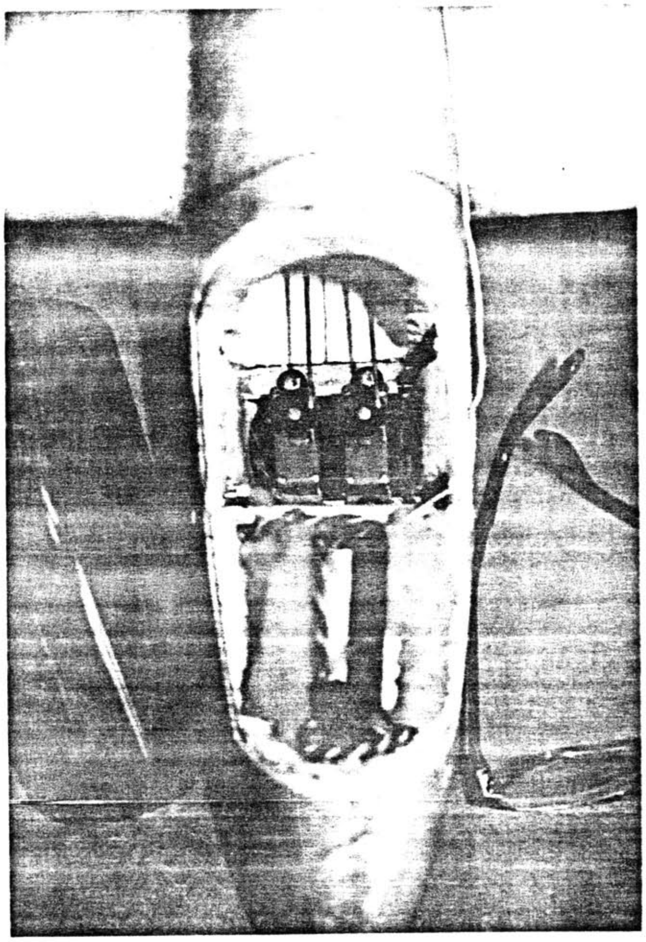

Fiberglass-epoxy covered wooden beams were attached to the fuselage beneath the wing. The yoke on the launcher bucket would push on these two beams to accelerate the glider during the launch phase. The beam and yoke interface is shown in Figure 8.

FIGURE 8

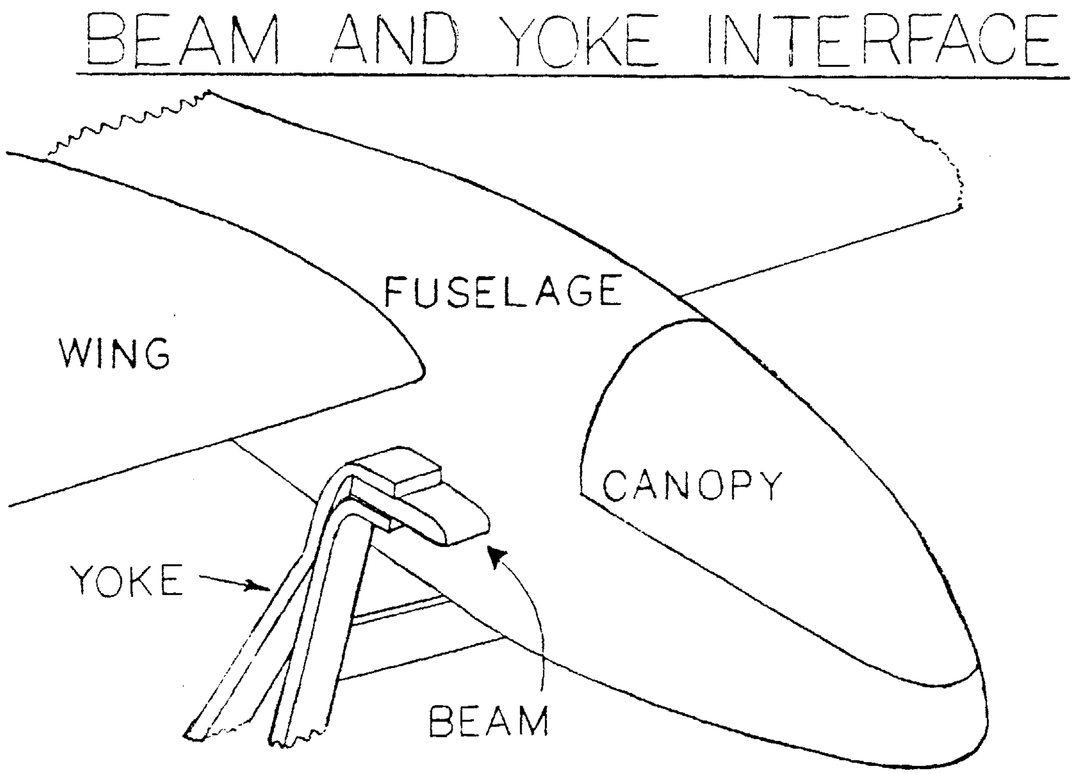

The yoke consisted of two parts; the front and the rear. The front section positioned the glider above the bucket so it would clear the launcher assembly upon take-off and transmitted the accelerative forced from the bucket to the glider. It had two triangular aluminum supports which attached to the bucket via the bucket's threaded tension rods. At the top front of these supports were two slots which fitted around the push beams on the glider. A slotted cross piece was screwed onto the back of the triangular pieces to allow for spacing of the supports. A schematic is shown in Figure 9.

FIGURE 9

FRONT YOKE

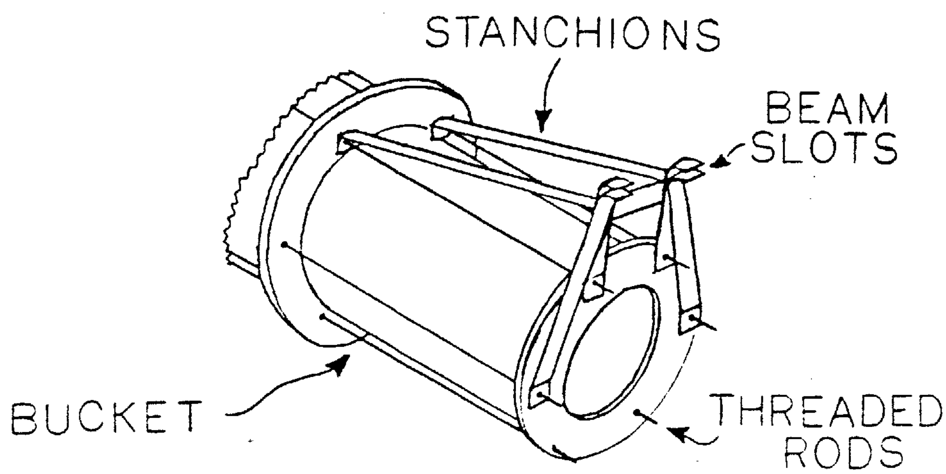

The rear section of the yoke was purely a vertical support piece to support the down load from the rear of the glider fuselage. This down load was created by the acceleration. Since the C.G. was above the push points, there was a moment creating a down load on the rear of the fuselage during acceleration, and the rear yoke transmitted this force to the rear of the bucket.

C) Structural and Stability Analysis - Dynamic Strength Testing

1) Structural Analysis

A simple structural analysis of the wing is carried out here to determine the operating limits of the Glider - Mark I.

Aircraft dimensional characteristics are given in Table 1.

TABLE 1

$b = 1.5$ m.	$S = 0.18$ m
$c = 0.12$ m	$W_g = 9.8$ Nt.
$t = 0.02$ m	$S_H = 0.033$ m
$AR = 12.5$	$S_V = 0.018$ m
$l_H = l_V = 0.43$ m	$W_w = 4.4$ Nt.

Fiberglass characteristics are given in Table 2.

TABLE 2

Fiber Properties		[+ 45] layup properties	
E_L = 70 gPa	F^L_{TU} = 3.4 gPa	F^L_{TU} = 1 gPa	E_L = 25 gPa
E_T = 17 gPa	F^T_{TU} = 150 mPa	F^T_{TU} = 1 gPa	E_T = 25 gPa
E_{12} = 2 gPa	F_{SU} = 200 mPa	F_{SU} = 200 mPa	E_{12} = 18 gPa
			z = 0.00018m

a) Wing Strength

Figure 10 shows modeling of the wing as a cantilever beam.

FIGURE 10

CANTILEVER BEAM MODEL OF WING

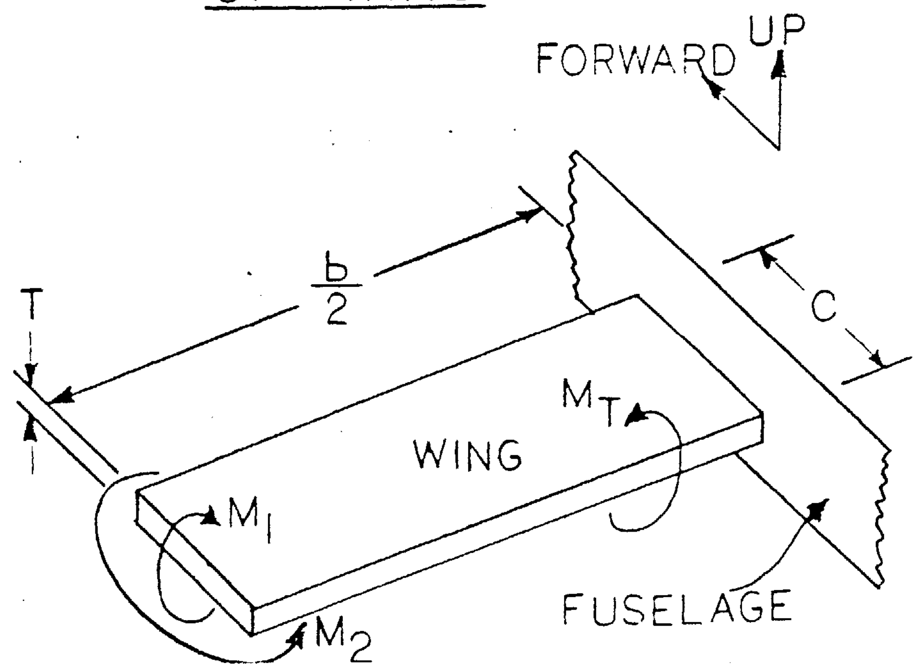

Equation (1) is a conservative determination of the moment on the wing at the root due to lift and is derived in Appendix B.

$$M_1 = \frac{W_g \left(AR / W_g / S \right)^{1/2}}{8} \, n_1 \, S.F._1 \qquad (1)$$

Equation (2) is a determination of the moment on the wing at the root due to acceleration, and is also derived in Appendix B.

$$M_2 = \frac{W_w\left[AR\, W_g / (W_g/S)\right]^{1/2}}{8} n_2\, S.F._2 \qquad (2)$$

with $S.F._1 = S.F._2 = 2$; $n_1 = 10$ (10 Gee pullup) ; $n_2 = 100$ (100 Gee acceleration)

we get $M_1 = 36.75$ Nt-m

$M_2 = 184$ Nt-m

If σ_{1max} and σ_{2max} are the stresses in the fiberglass skin at the root of the wing due to M and M respectively, these are given (from simple beam theory) by:

$$\sigma_{1max} = \frac{M_1\, t/2}{I_1} \qquad (3)$$

$$\sigma_{2max} = \frac{M_2\, c/2}{I_2} \qquad (4)$$

for this wing: $\sigma_{1max} = 44$ mPa

$\sigma_{2max} = 27$ mPa

These are both well below the allowable 200 MPa.

The maximum allowable M is given by:

$$M_{1max} = \frac{F_{Tu}^{f}\ I_1}{t/2} \qquad (5)$$

this is: $M_{1max} = 170$ Nt-m

Since it is unclear what the response of the glider will be when leaving the launcher, it is necessary to calculate the maximum allowable speed the glider may be launched at if it comes off the launcher at $C_L = C_{L_{max}}$.

since: $$L = 1/2\ \rho_{air} V^2 C_{L_{max}} S \tag{6}$$

and: $$M_l = \frac{L/b\,(b/2)^2}{2} \tag{7}$$

we can combine (6) and (7) to solve for V_{max} in terms of $M_{l_{max}}$, and get:

$$V_{max} = \left[\frac{8\ M_{l_{max}}}{3\,\rho_{air}\ C_{L_{max}}\ S} \right]^{1/2} \tag{8}$$

so: $V_{max} = 83$ m/sec

The torsional moment M_T is a combination of that from lift and that from the moment coefficient of the wing. Figure 11 shows the model of the wing to be used.

FIGURE 11

WING TORSION MODEL

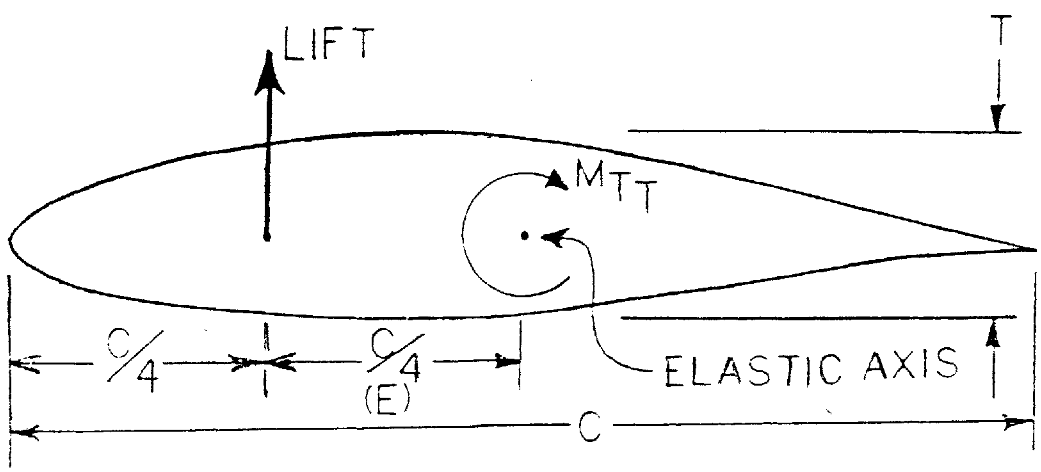

with : A = 0.00144 m (cross sectional area)

C_m = -0.1

h = 2z = 0.00036 m

$$M_{T_{max}} = M_{T_T} + M_{T_L} = \frac{1}{2} \rho_{air} V_{max}^2 \left(c\, C_m + \frac{1}{4} c\, C_{L_{max}} \right) S \qquad (9)$$

$$M_{T_{max}} = 0.0053\, V_{max}^2$$

The stress in the wing skin is given by:

$$\sigma_{12_{max}} = \frac{M_{T_{max}}}{2Ah} \qquad (10)$$

Letting $\sigma_{12} = F_{su}$ and solving for V_{max} by combining (9) and (10):

$$V_{max} = \left[\frac{2Ah\ F_{su}}{\frac{1}{2} \rho_{air} S c \left(C_m + \frac{1}{4} C_{L_{max}} \right)} \right]^{1/2} \qquad (11)$$

or: $V_{max} = 200$ m/sec

This is well above any planned or even reachable velocity.

b) Wing Stiffness

The torsional inertia of the wing is given by:

$$J = \frac{4A^2}{\oint \frac{ds}{h}} \qquad (12)$$

where ds is the circumference of the wing in the chord direction.

The maximum angle of twist of the wing is given by:

$$\theta_{max} = \frac{M_{T_{max}}\ b/2}{2 E_{12/2}\ J} \qquad (13)$$

so at $V = 80$ m/sec. :

$\theta_{max} = 4.3^{\circ}$

The divergent dynamic pressure of the wing is given by:

$$q_D = \tfrac{1}{2}\rho_{air} V_D^2 = \frac{\pi^2 E_{1212} J \frac{\partial C_L}{\partial \alpha}}{4(b/2)^2 c e} \qquad (14)$$

where $\frac{\partial C_L}{\partial \alpha} \approx 5.4$ and is derived in Appendix D.
Then the divergent speed is:

$$V_D = \left[\frac{\pi^2 E_{1212} J}{2(b/2)^2 \rho_{air} c e \frac{\partial C_L}{\partial \alpha}}\right]^{1/2} \qquad (15)$$

$$V_D \approx 250 \text{ m/sec} \qquad (\sim 550 \text{ mph})$$

Again, this is well above any planned or reachable velocity.

It has been shown through these simple estimations of the wing strength and stiffness that the Glider-Mark I should be capable of withstanding the inertial and aerodynamic loads imposed upon it by the electromagnetic launch and subsequent flight. To test the response to inertial loading, the Glider-Mark I was placed on the yoke structure on the bucket and held in place with strapping tape. The bucket was fired repeatedly to a velocity of 15 m/sec. at average accelerations varying from 200 m/sec./sec. (~20 Gee) to 2500 m/sec./sec. (~250 Gee). The peak acceleration reached (albeit for a very short time - approximately two milliseconds) was 4000 m/sec./sec. (~400 Gee).

No damage to either the aircraft structure or the radio control components was noted. Since the peak acceleration expected on launch would be 2000 m/sec./sec. (~200 Gee) maximum, the glider was deemed acceptably strong with regard to inertial loading, having at least a safety factor of two.

2) Stability Analysis

a) Longitudinal Static Stability

Using the derivations in Appendix C, the Data in Table 1, and the following data in Table 3:

TABLE 3

Center of Gravity:	$X_{C.G.} = 0.05$ m
Wing Aerodynamic Center:	$X_{A.C.} = 0.027$ m
Wing Lift Curve Slope:	$a = 5.4$
Horiz. Tail L. C. S.:	$a_1 = 3.0$
Elevator Lift Curve Slope:	$a_2 = 2.0$
Tail Incidence Angle:	$\eta_T = 0$
Change in Downwash:	$\frac{\partial \epsilon}{\partial \alpha} = 0.2$
Moment Coefficient:	$C_{m_0} = -0.1$

The following can be calculated:

Horizontal Tail Lift:

$$L_{horiz.Tail} = -0.0031\ V^2 + 0.525$$

Horizontal Tail Lift Coefficient:

$$C_{L_{horiz.\ Tail}} = -0.1533 + 25.97/V^2$$

Elevator Angle to Trim:

$$\eta = 0.544\ C_{L_{horiz.\ Tail}} - 0.23\ C_L$$

Tail Incidence Angle:

$$\alpha_T = 0.333\ C_{L_{horiz.\ Tail}} - 0.666\ \eta$$

These are tabulated for various flight speeds in Table 4.

TABLE 4

Velocity m/sec.	C_L	$C_{L_{horiz.\ Tail}}$	η rad	α_T rad
10	0.84	0.106	-0.147	0.133
30	0.099	-0.124	-0.090	0.019
50	0.036	-0.143	-0.085	0.010
70	0.018	-0.148	-0.084	0.007
90	0.011	-0.150	-0.083	0.006

The stick fixed neutral point is:

$$h_n = 0.495$$

so the static margin:

$$K_n = 0.078$$

This is positive, so the aircraft is longitudinally statically stable.

b) Longitudinal Dynamic Stability

The longitudinal dynamic stability derivatives and dimensional parameters (as derived in Appendix D) are listed in Table 5. The ones that have a lift coefficient dependence are given for each velocity.

TABLE 5

Derivative	Value
a	5.4
C_{L_α}	5.84
C_{m_α}	-0.421
C_{z_α}	-5.84
C_{x_u}	-0.03
C_{z_q}	-3.65
C_{m_q}	-13.08
$C_{z_{\dot\alpha}}$	0.73
$C_{m_{\dot\alpha}}$	-2.61
i_B	975
μ	76
l	0.06

	10 m/sec	50 m/sec	80 m/sec
C_L	0.89	0.036	0.014
C_{x_α}	0.278	0.111	0.0043
C_{z_u}	0.001	0.001	0.001
t^*	0.006	0.0012	0.00075

Using the approximate solutions in Appendix E, values for the natural frequency and damping ratio in both the Phugoid and Short Period Modes are obtained.

i) Phugoid mode	10 m/sec	50 m/sec	80 m/sec
nat. freq. (rad/sec)	0.0083	0.000335	0.00013
damping ratio	0.012	0.29	0.76
period (sec.)	4.6	23.5	55.8
halving time	41.6	8.5	5.2
Cycles to halve	9.0	0.36	0.09

ii) Short Period Mode	10 m/sec	50 m/sec	80 m/sec
nat. freq. (rad/sec)	0.031	0.031	0.031
damping ratio	0.88	0.88	0.88
period (sec.)	2.7	0.52	0.34
halving time	0.15	0.03	0.019
cycles to halve	0.057	0.057	0.057

It is seen that the aircraft is stable in both Phugoid and Short period mode oscillations, with the stability in the Phugoid mode actually increasing with increasing velocity.

C) Lateral Dynamic Stability

The lateral dynamic stability derivatives and dimensional parameters (as derived in Appendix D) are listed in Table 6. The ones that have a lift coefficient dependence are given for each velocity.

TABLE 6

derivative	value
C_{y_β}	-0.2
C_{y_p}	0
C_{ℓ_p}	-0.385
C_{y_r}	0.115
μ	6.05
l	0.75
i_A	1.02
i_C	1.45
i_E	0.014

	10 m/sec	50 m/sec	80 m/sec
C_{n_β}	0.05	0.0443	0.0443
C_{ℓ_β}	-0.043	-0.018	-0.017
C_{n_r}	-0.055	-0.038	-0.037
C_{ℓ_r}	0.033	0.012	0.011
C_{n_p}	-0.066	0.002	0.0035
t^*	0.075	0.015	0.0094

Using the exact solution in Appendix E for lateral motion, the characteristic equation is obtained for each velocity. Solving the characteristic equation gives the following roots:

TABLE 7

roots	10 m/sec	50 m/sec	80 m/sec
λ_1	-0.00213	-0.000025	-0.00001
λ_2	-0.395	-0.378	-0.375
$\lambda_{3,4}$	$-0.017\pm0.204i$	$-0.021\pm0.174i$	$-0.022\pm0.171i$

The characteristics of the lateral dynamics are given in Table 8.

TABLE 8

Dutch Roll	10 m/sec	50 m/sec	80 m/sec
period (sec)	2.31	0.542	0.345
halving time	3.06	0.49	0.29
cycles to halve	1.32	0.91	0.84
Spiral Mode			
halving time	24.3	414	667
Rolling mode			
halving time	0.13	0.027	0.017

It can be seen that the aircraft is laterally stable in all modes, although the spiral instability takes a very long time to damp out at high speeds.

The stability of the Glider - Mark I has been confirmed at all velocities in all of the lateral and longitudinal modes. The next step was the flight testing.

D) Flight Testing - Conventional Launches (Strake Addition)

Prior to an electromagnetic launch, it was deemed appropriate to launch the glider by conventional means (Hi-Start) to determine its operating and flight characteristics. On a cold Saturday morning in March 1981 Jorge Chavier and I took the plane, Hi-Start, and radio control equipment out onto Briggs Field at M.I.T. The elevator and rudder were adjusted by eye, and then a few hand launches were performed to get the final trim settings. The glider flew smoothly and slowly with few adjustments, and then a Hi-Start launch was attempted.

The Hi-Start launcher consists of 130 meters of nylon fishing line and 30 meters of surgical grade rubber tubing. One end of the nylon line is staked down, the tubing tied to the other end, and the free end of the tubing hooked onto the glider tow hook. The rubber tubing is stretched, and the system functions as a huge slingshot. A representation of the launch process is shown in Figure 12.

FIGURE 12

HI-START LAUNCH

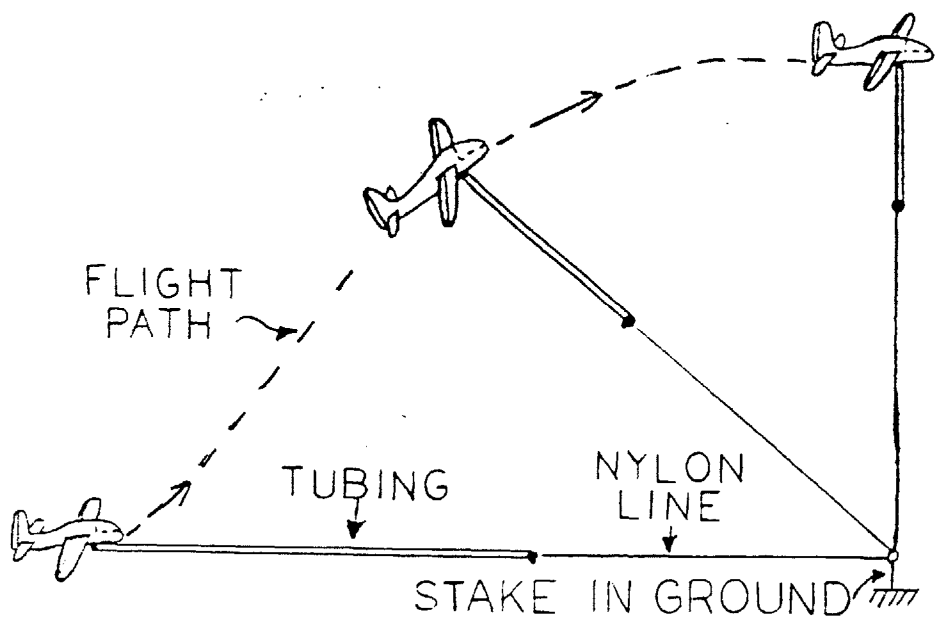

We launched the glider twice with the Hi-Start. It was determined (by Jorge) that there was a pronounced tendency to turn left, and the vertical stabilizer wasn't very effective, although the rudder was. During the following week modifications to the vertical stabilizer (adding a strake) and to the right wing (adding some washout) were performed to alleviate the deficiencies. The next Saturday we Hi-Start launched the glider two more times. The stabilizer was more effective and the tendency to turn left was eliminated. The glider showed no other adverse flight characteristics, and was deemed ready for electromagnetic launching.

E) Flight Testing - Electromagnetic Launches

Four electromagnetic launches were performed in late March 1981. Everyone in the Accelerator group helped bring all the equipment out to Briggs Field on a rented truck. We set up the launcher at approximately a 20 degree angle (resting one end on a fence). The charging circuit and capacitor banks were kept in the truck, and were plugged into an outlet near the M.I.T. solar house. Jorge hand launched the glider a few times to check the trim and we placed the glider in the yoke on the bucket. Two of the capacitor banks were charged up to 140 volts. We waited until the air was calm and then the banks were discharged, launching the glider at a velocity of approximately 30 m/sec. The average acceleration was 200 m/sec/sec (20 Gees) and the peak acceleration was twice that. The glider went straight ahead at an angle of 20 degrees to an altitude of about 25 meters where Jorge leveled it off and flew two large, fast left hand circles. He then brought the glider in for a perfect landing 10 meters from the launcher. Jorge and I examined the plane and radio, deemed them airworthy, and the glider was put on the launcher yoke again. The two banks were charged to 160 volts, and when the air again became calm, the banks were discharged, launching the glider at a velocity of 35 m/sec. The average acceleration was 250 m/sec/sec (25 Gees) and the peak acceleration was twice that. The glider again went straight ahead to an altitude of 35 meters. Jorge flew it in a few circles but it landed hard since the wind had picked up. The tail was cracked and the nose was dented, but those were both patched up with fiberglass and epoxy that night.

The next time we brought the launcher out to Briggs Field we also brought an A-frame to lift the end of the launcher to four meters off the ground, making the angle of launch about 40 degrees. The glider was placed on the yoke, and three banks were charged to 160 volts. When the banks were discharged the glider climbed at a 40 degree angle to approximately 55 meters altitude. The launch velocity was 40 m/sec., with an average acceleration of 300 m/sec/sec. Jorge flew it for about 45 seconds and then brought it in for a landing. After another examination we put the glider on the yoke and charged the three banks to 200 volts. The discharge launched the glider at a 40 degree angle at 45 m/sec. The average acceleration was 500 m/sec/sec. The glider climbed to 75 meters altitude but then Jorge had a partial control loss, and a mild crash resulted. That concluded the Glider Mark I electromagnetic launches. Figure 13 shows the launcher at 20 degrees for the first two launches, and Figure 14 shows the launcher at 40 degrees for the last two launches.

FIGURE 13

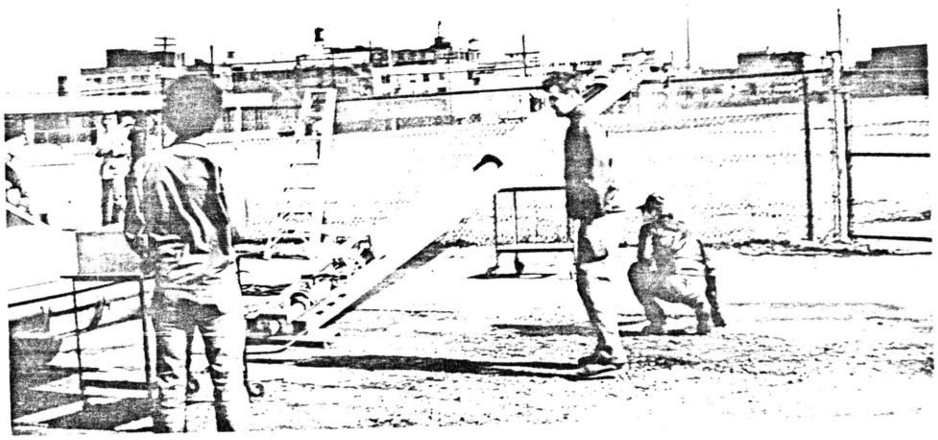

FIGURE 14

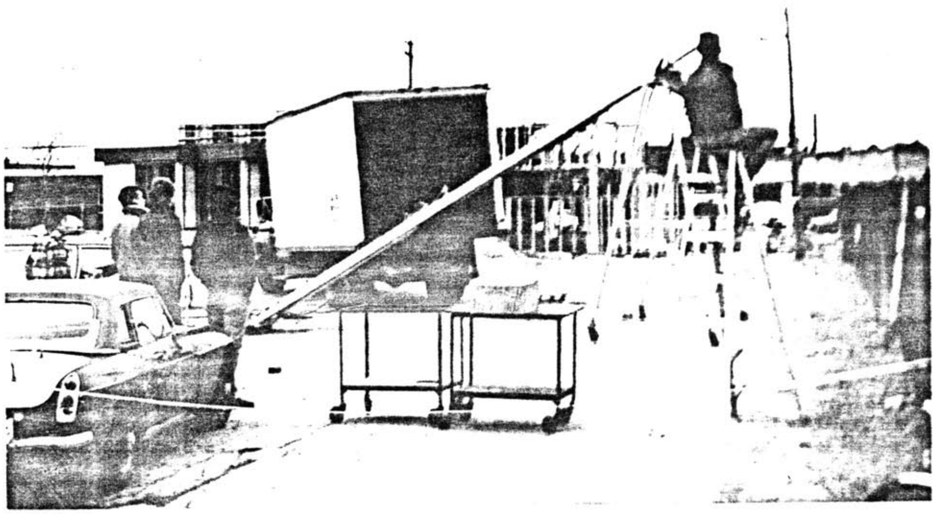

Table 9 includes launch angle, altitude, velocity, accelerations, bank voltages, and number of banks used.

TABLE 9

launch	#banks	Volts	angle	alt. (m.)	speed	acceleration (m/sec^2) avg.	acceleration (m/sec^2) peak
1	2	140	20	25	30	200	400
2	2	160	20	35	35	250	500
3	3	160	40	55	40	300	600
4	3	200	40	75	45	500	1000

With its glide ratio of approximately fifteen, this glider could have flown one to one and a half kilometers had it gone in a straight line, from an altitude of 75 meters and a launch velocity of 45 m/sec.

V. GLIDER - MARK II DESIGN: CARGO GLIDER

A) Preliminary Design and Configuration Determination

The Glider - Mark II was to be a half scale model of the 22 kilogram cargo glider. Therefore the general layout and design of the cargo glider had to be determined before the half scale model could be designed. A modular system would be used, allowing for easy and compact transportation and assembly in the support area. There would be a fuselage cargo compartment with snap-in snap-out cargo pods and a removable wing for compactness during storage.

Since the aircraft is a glider, the glide ratio (or lift-to-drag ratio) is a very important factor in determining the effectiveness of the craft. The higher the glide ratio, the farther the glider can fly from a given altitude. In this case, the higher the glide ratio the better. The L/D (lift-to-drag ratio) is a function of many things, the main ones being two features of the aircraft configuration; the aspect ratio (length to width ratio of the wing) and the wing loading (the weight of the aircraft divided by the wing planform area). For any specific configuration it is also a function of the flight velocity.

A graph of $(L/D)_{max}$ vs. Aspect Ratio for different wing loadings is given in Figure 15. This is for different wings on an arbitrary fuselage.

FIGURE 15

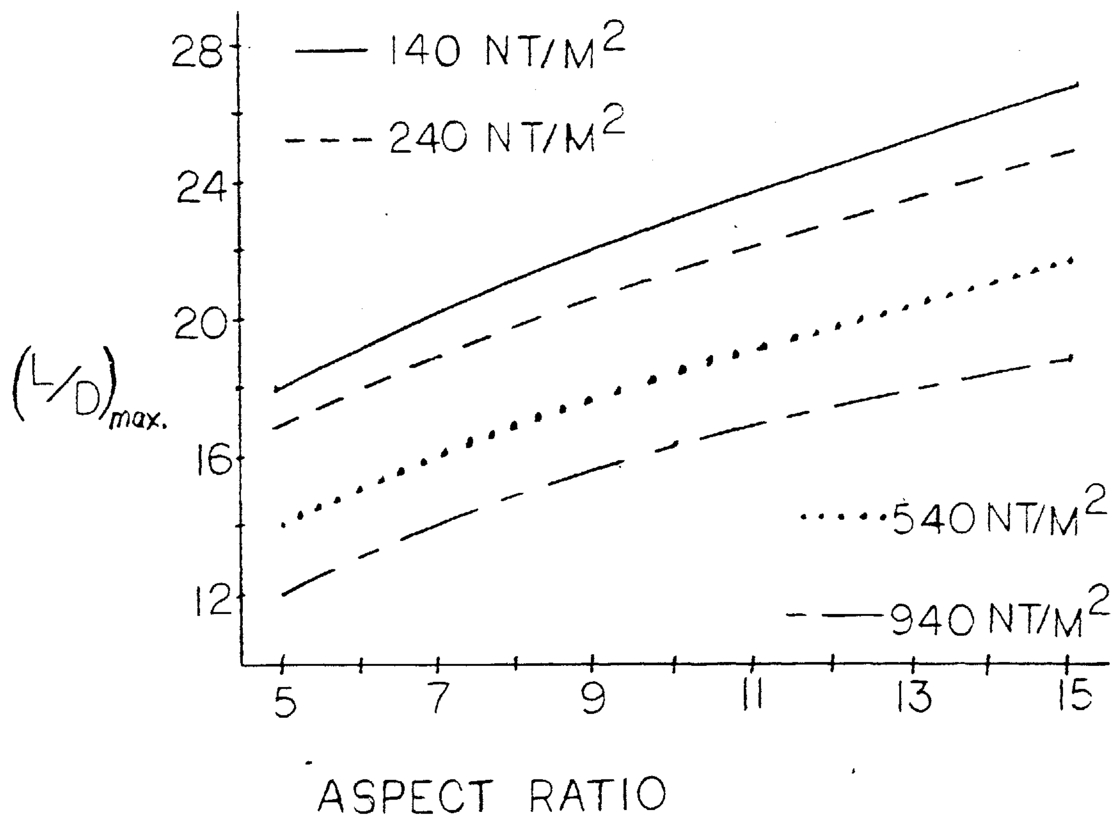

It is seen that the $(L/D)_{max}$ increases with increasing aspect ratio and decreases with increasing wing loading. The increase with AR (aspect ratio) is caused by a reduction in the induced drag at high AR's, and as the drag goes down while the lift remains constant, the L/D rises. An increase in the wing loading (with the same fuselage) entails a smaller wing. Since the fuselage is the same size but the wing is smaller, the ratio of fuselage drag to wing drag increases, thereby causing a decrease in the L/D.

The L/D is also a function of the flight velocity, and a graph of sink velocity vs. forward velocity is given in Figure 16. This graph is commonly known as a drag polar.

FIGURE 16

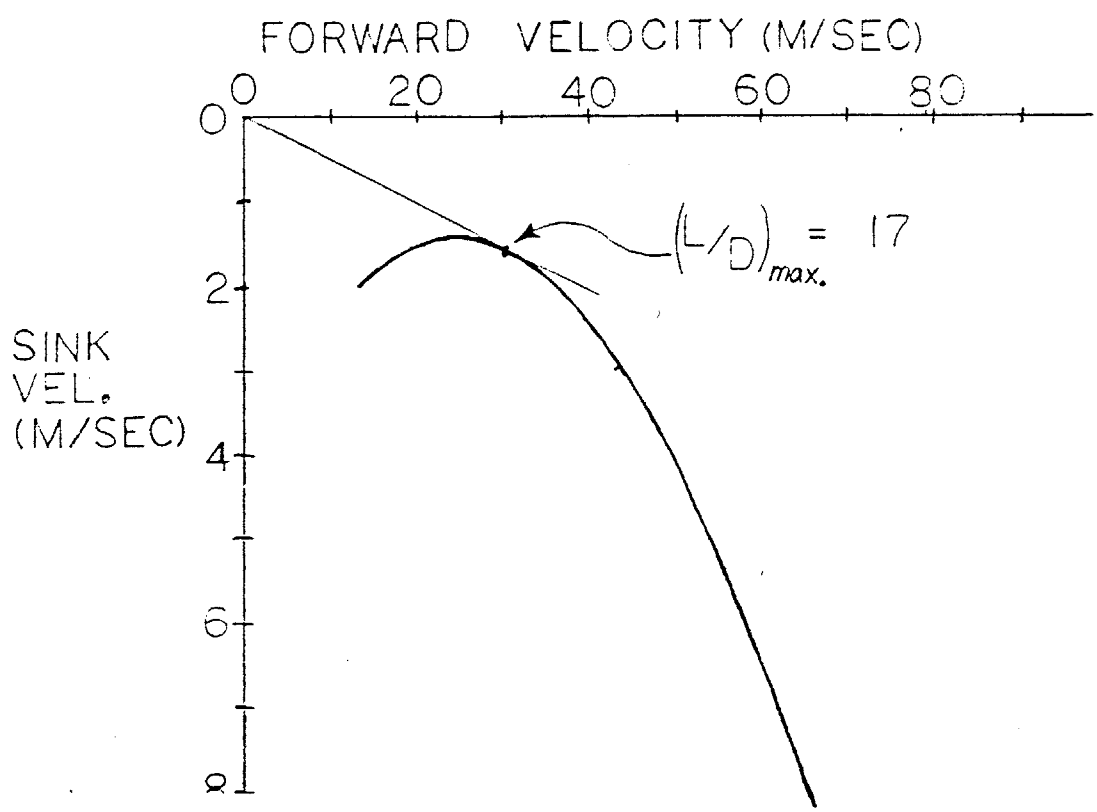

It is seen that the point where a tangent line through the origin touches the curve must be the point of $(L/D)_{max}$, and that the forward velocity divided by the sink velocity is the L/D.

A large high AR wing by necessity weighs more than a small low AR wing, and therefore subtracts from the cargo carrying capacity of the glider even as it increases its range. It was determined that a wing loading of 200 Nt/m^2 and an aspect ratio of about 15 would give a payload to gross weight ratio of approximately 1/2 (good for a glider) and also give the requisite range capability.

B) Final Configuration

A view of the final configuration of the 1/2 scale Cargo Glider Mark II is seen in figure 17.

FIGURE 17

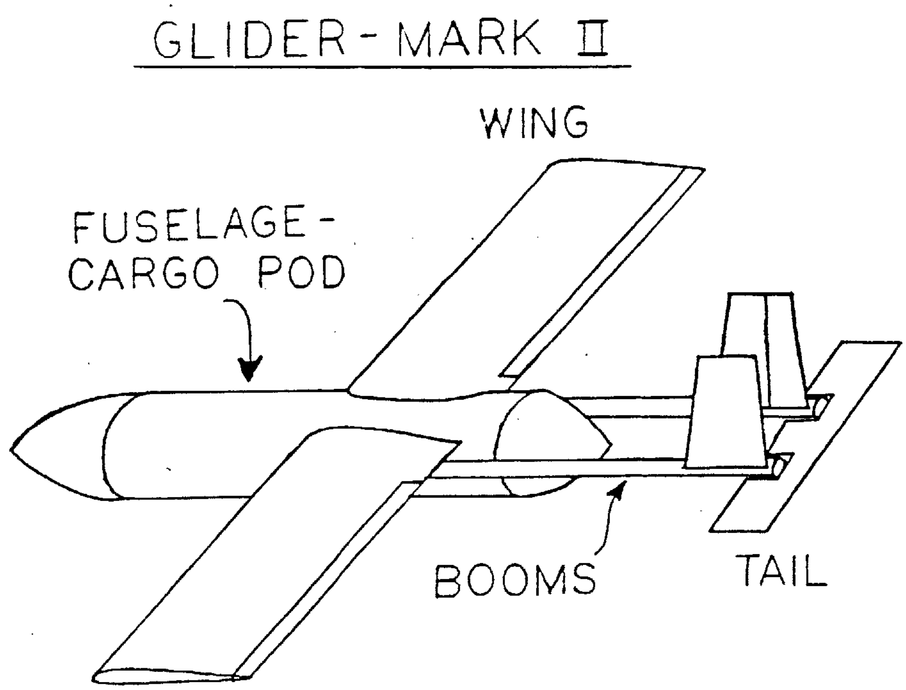

It is a pod and twin boom configuration, with twin vertical stabilizers and an all flying horizontal stabilizer. It has 3-axis control (elevator, rudder, ailerons). The reason for this design is its modularity. The wing, fuselage, and tail and boom assemblies can be constructed separately and then bolted together. This would be convenient in the field, as a stock of the three components could be stored and then put together just before the flight, saving a great deal of space. It is also a convenient design for the construction and testing phases of the program. It allows the construction of replacement parts which can just be bolted in place in case of a damaging crash. This would save time and also allow assembly line procedures in the construction.

The Glider - Mark II characteristics are given in Table 10.

TABLE 10

Gross Weight	W_g	55.7 Nt.
Empty Weight	W_e	22 Nt.
Wing Area	S	0.28 m.
Horizontal Tail Area	S_H	0.05 m.
Vertical Tail Area	S_V	0.034 m.
Fuselage Length	F_L	0.6 m.
Fuselage Diameter	w	0.13 m.
Boom Length	l_V	0.43 m.

		Short Wing	Long Wing
Aspect Ratio	AR	6	12
Span	b	1.29 m.	1.82 m.
Chord	c	0.22 m.	0.15 m.

Two wings have been planned; an aspect ratio of 6 and an aspect ratio of 12. The low aspect ratio wing is a conservative wing, stronger and more stable (as will be shown later), although with lower performance. It will be used first to prove out the glider and then the longer wing will be used to obtain a longer range.

C) Materials Selection

1) Wing

As in the Glider - Mark I a foam core fiberglass-epoxy skin would be used. This is stronger, lighter and simpler than a built up wing. The foam is 30 kg/m^3 density blue construction insulation styrofoam. The fiberglass used is 0.2 kg/m^2 90 degree weave cloth, with Hobbypoxy 2 epoxy.

The ailerons are heavy balsa wood, as are the wing tips. Pine blocks under the skin are used as fuselage attachment points.

2) Fuselage

Standard model aircraft construction techniques were chosen for simplicity and familiarity reasons. Spars would be spruce, while the bulkheads would be plywood. The frame would be skinned with 1/16" balsa sheet and then covered with one layer of fiberglass-epoxy. The nose and tail cones would be carved from the styrofoam insulation and then covered with one layer of fiberglass-epoxy.

3) Tail and Booms

The tail (both horizontal and vertical stabilizers) would be shaped from hard balsa and then covered with one layer of fiberglass-epoxy. This provides more than adequate strength and stiffness, and is simple to build.

The booms would be aluminum tubes, chosen for their stiffness. Fiberglass-epoxy tubes would be better (having a higher stiffness to weight ratio) however they weren't available at construction time. The penalty was a little weight. The boom tubes would have pine plugs in them at areas of stress concentration.

D) Structural Analysis

The structural analysis concerns the main aircraft components, i.e. the wing, fuselage, booms, and tail. It uses simple beam theory and torsion theory, along with idealized simplifications of the actual structure. However, all the simplifications and idealizations are conservative ones, giving results lower in strength and stiffness than will actually be the case.

Wing Strength

Using the Data in Table 2, Table 10 and the modeling in Figure 10; following through the analysis given in equations one through eight in Chapter IV, a maximum velocity at $C_{L_{max}}$ is obtained for both the long and short wings. These maximum velocities are:

short wing: $V_{max} \approx 85$ m/sec (~210 mph)

long wing: $V_{max} \approx 80$ m/sec (~200 mph)

The maximum allowable velocity from torsional moments is found using Figure 11 and equations nine through 11 (in Chapter IV). These maximum velocities are:

short wing: $V_{max} \approx 400$ m/sec (~900 mph)

long wing: $V_{max} \approx 375$ m/sec (~850 mph)

Because these have been very conservative estimates of the strength of the wing in bending and in torsion, it is seen that the glider can withstand any planned velocity even at $C_{L_{max}}$.

2) Wing Stiffness

Using the formulation given in Chapter IV equations 12 through 15, the divergent speed and maximum twist of the wings are found. These are:

short wing: V_D = 400 m/sec (~900 mph)

α_{max} = 2.6 degrees @ 80 m/sec

long wing: V_D = 350 m/sec (~780 mph)

α_{max} = 2.5 degrees @ 80 m/sec

Again, the wing stiffness is adequate for any reachable velocities.

3) Fuselage Strength

The fuselage stringers must be capable of withstanding the full accelerative forces the glider will feel while being launched. To be conservative, it is assumed that the stringers will see the full weight of the glider at 100 gees with a safety factor of two. Spruce properties are listed below:

ρ = 450 kg/m

E = 9.6 gPa

F_{TU} = 69 mPa

The total area for the stringers is given by

$$A = \frac{F}{F_{TU}} \tag{16}$$

where F is the total force. In this case

$$F = W_g\, n_1\, S.F._1 \tag{17}$$

so

$$A = \frac{W_g\, n_1\, S.F._1}{F_{TU}} \tag{18}$$

substituting:

$$A = 23 \text{ mm}^2$$

With eight square stringers, each must be 4.7 mm. on a side.

4) Boom Strength and Stiffness

Stresses in the tail booms will be produces by moments from the aerodynamic forces of the tail and by accelerative loads applied by the launcher. If the total boom and tail weight is assumed to be 1/10 the gross weight of the glider, then with the following properties in Table 11,

TABLE 11

Aluminum		Boom Dimensions	
ρ	= 2800 kg/m.	l_v	= 0.43 m.
E_n	= 72 gPa	O.D.	= 2.86 cm.
F_{TU}	= 440 mPa	wall thickness	= 0.89 mm.
		W_{b+T}	= 5.6 Nt.

the stress due to acceleration is:

$$\sigma_a = 14.3\ mPa$$

And the stress due to tail forces, assuming $C_{L_{max}}$ = 1.2 and V = 80 m/sec:

$$\sigma_{T_f} = 45\ mPa$$

Both of these are well below the yield stress of aluminum of 440 mPa.

It was required to keep the bending of the tail booms as low as possible to minimize the unwanted angular deflections of the tail. A deflection of one degree at the tail was allowable. The deflection of the tail (modeled as a clamped cantilever beam) from simple beam theory is:

$$f_{max} = \frac{F\, l_v^3}{3 E_n I} \qquad (19)$$

where F is the down (or up) force from the tail and I is the moment of inertia of both booms.

$$F = \tfrac{1}{2} \rho_{air} V^2 C_{L_{Tail}} S_H \qquad (20)$$

$$I = \frac{\pi}{4}\left[\left(\frac{O.D}{2}\right)^4 - \left(\frac{O.D.}{2} - \text{wall thickness}\right)^4\right] \qquad (21)$$

Substituting (20) and (21) into (19), after inserting the proper values we get:

$$f_{max} = 0.75 \text{ cm.}$$

over the 43 cm. length of the booms this is a deflection of approximately one degree, and as such is acceptable.

5) Tail Strength

The tail must withstand the inertial accelerative forces imposed upon it by the launch, and also the maximum aerodynamic loads that might be encountered.

The maximum lift (either positive or negative) produced by the horizontal stabilizer is:

$$F = 200 \text{ Nt.}$$

so the lift distribution is:

$$w_H = 447 \text{ Nt/m.}$$

The maximum moment will be where the outer sections of the stabilizer meet the tail booms. then:

$$M_{I_{max}} = W_H \frac{\left(b_H/3\right)^2}{2} = 4.96 \text{ Nt-m.}$$

For the fiberglass-epoxy covered horizontal stabilizer, the moment of inertia about the Y-axis is:

$$I = 800 \times 10^{-12} \ m^4$$

Then the maximum stress in the stabilizer will be:

$$\sigma_a = MY/I = 30 \ mPa$$

This is well below the ultimate strength of the fiberglass of 200 mPa.

From acceleration, the maximum moment will be:

$$M_{z_{max}} = 5 \ Nt\text{-}m$$

The moment of inertia about the Z-axis is:

$$I = 8.5 \times 10^{-9} \ m^4$$

Then the maximum stress will be:

$$\sigma_I = 30 \ mPa$$

A similar analysis is carried out for the vertical stabilizers, and gives a maximum stress from aerodynamic loads of:

$$\sigma_a = 20 \ mPa$$

And a maximum stress from inertial loading of:

$$\sigma_I = 21 \text{ mPa}$$

It is seen that all of these stresses are well below the maximum allowable stress in the fiberglass of 200 mPa.

This analysis has shown that all the major structural components are capable of withstanding any and all loads that may be encountered either be aerodynamic loading or by inertial loading.

E) Stability Analysis

1) Longitudinal Static Stability

Using the same methods as for the Glider - Mark I, we use the aircraft characteristics given in Table 10 along with the following data in Table 12:

TABLE 12

	empty weight	gross weight
h_1	0.356	0.231
h_0	0.225	0.225
a(long wing)	5.4	5.4
a(short wing)	4.71	4.71
a_1	3.0	3.0
a_2	2.0	2.0
η_T	0	0
$\frac{\partial \epsilon}{\partial \alpha}$	0.2	0.2
C_{m_0}	-0.1	-0.1

We can now compute h_n (the stick fixed neutral point):

short wing: $h_n = 0.372$

long wing: $h_n = 0.392$

And the Static margin K_n :

		empty weight	gross weight
long wing:	K_n	0.016	0.141
short wing:	K_n	0.036	0.161

All of these are positive, so the aircraft will be longitudinally statically stable with either wing, either empty or at gross weight.

2) Longitudinal Dynamic Stability

The longitudinal dynamic stability derivatives and dimensional parameters (as derived in Appendix D) for the Glider - Mark II with either wing at gross weight and at empty weight are given in table 13.

TABLE 13

	short wing		long wing	
Derivative	empty	gross	empty	gross
a	4.71	4.71	5.4	5.4
C_{L_α}	5.13	5.13	5.8	5.8
C_{m_α}	-0.075	-0.664	-0.086	-0.761
C_{z_α}	-5.13	-5.13	-5.8	-5.8
C_{x_u}	-0.03	-0.03	-0.03	-0.03
C_{z_q}	-1.962	-1.962	-1.986	-1.986
C_{m_q}	-3.90	-3.90	-3.95	-3.95
$C_{z_{\dot\alpha}}$	-0.393	-0.393	-0.393	-0.393
$C_{m_{\dot\alpha}}$	-0.78	-0.78	-0.79	-0.79
i_B	65	408	430	1070
μ	60	150	85	213
l	0.108	0.108	0.076	0.076

short wing

	empty		gross	
	25 m/sec	100 m/sec	25 m/sec	100 m/sec
C_L	0.2	0.013	0.51	0.031
C_{X_α}	0.08	0.005	0.204	0.013
C_{Z_u}	-0.0012	-0.0013	-0.0032	-0.0031
t^*	0.00432	0.00108	0.00432	0.00108

long wing

	empty		gross	
	25 m/sec	100 m/sec	25 m/sec	100 m/sec
C_L	0.2	0.013	0.51	0.031
C_{X_α}	0.135	0.0088	0.345	0.021
C_{Z_u}	-0.0012	-0.0013	-0.0032	-0.0031
t^*	0.00304	0.00076	0.00304	0.00076

Using the approximate solutions in Appendix E, values for the natural frequency, damping ration, period, halving time and cycles to halve are obtained.

i) Phugcid Mcde

short wing

	empty		gross	
	25 m/sec	100 m/sec	25 m/sec	100 m/sec
ω_n (rad/sec)	0.0023	0.00015	0.0024	0.00015
ζ	0.053	0.815	0.021	0.342
T (sec)	11.75	78	11.75	48
t_{half} (sec)	24.4	6.1	59.6	14.9
N_{half}	2.1	0.08	5.1	0.31

long wing

	empty		gross	
	25 m/sec	100 m/sec	25 m/sec	100 m/sec
ω_n (rad/sec)	0.0017	0.00011	0.0017	0.0001
ζ	0.053	0.816	0.02	0.342
T (sec)	11.5	75.1	11.25	49.1
t_{half} (sec)	23.8	5.84	61.7	14.9
N_{half}	2.1	0.08	5.5	0.3

ii) Short Period Mode

short wing

	empty		gross	
	25 m/sec	100 m/sec	25 m/sec	100 m/sec
ω_n (rad/sec)	0.038	0.038	0.042	0.042
ζ	0.929	0.929	0.338	0.338
T (sec)	0.073	0.018	0.068	0.017
t_{half} (sec)	0.083	0.021	0.21	0.052
N_{half}	0.86	0.86	0.31	0.31

long wing

	empty		gross	
	25 m/sec	100 m/sec	25 m/sec	100 m/sec
ω_n (rad/sec)	0.014	0.014	0.026	0.026
ζ	0.495	0.495	0.327	0.327
T (sec)	1.59	0.398	0.77	0.19
t_{half} (sec)	0.3	0.076	0.247	0.062
N_{half}	0.19	0.19	0.32	0.32

It is seen that the aircraft is stable in both the Phugoid and Short Period Mode oscillations at either speed with either wing. This confirms the longitudinal Dynamic Stability.

3) Lateral Dynamic Stability

The lateral dynamic stability derivatives and dimensional parameters (as derived in Appendix D) for the Glider - Mark II with either wing at gross weight and at empty weight are given in Table 14.

TABLE 14

	short wing		long wing	
Derivative	empty	gross	empty	gross
C_{Y_β}	-0.233	-0.233	-0.233	-0.233
C_{Y_p}	0	0	0	0
C_{ℓ_p}	-0.23	-0.23	-0.36	-0.36
C_{Y_r}	0.155	0.155	0.113	0.113
μ	10	25.1	7.3	18.36
l	0.645	0.645	0.91	0.91
i_A	0.707	1.767	0.3112	0.778
i_C	1.162	2.904	.468	1.17
i_E	0.025	0.064	0.011	0.026

short wing

	empty		gross	
	25 m/sec	100 m/sec	25 m/sec	100 m/sec
C_{n_β}	0.0573	0.057	0.059	0.057
C_{l_β}	-0.038	-0.029	-0.054	-0.030
C_{n_r}	-0.059	-0.058	-0.063	-0.058
C_{l_r}	0.014	0.009	0.022	0.010
C_{n_p}	-0.0013	0.008	-0.017	0.007
t^*	0.026	0.0065	0.026	0.0065

long wing

	empty		gross	
	25 m/sec	100 m/sec	25 m/sec	100 m/sec
C_{n_β}	0.041	0.040	0.042	0.040
C_{l_β}	-0.205	-0.201	-0.215	-0.201
C_{n_r}	-0.032	-0.032	-0.034	-0.032
C_{l_r}	0.059	0.008	0.145	0.013
C_{n_p}	-0.006	0.004	-0.021	0.003
t^*	0.0364	0.0091	0.0364	0.0091

Using the exact solutions in Appendix E for lateral motion, a characteristic equation is obtained for each set of derivatives (the glider with each wing at each velocity). Using the roots of these characteristic equations to obtain the flight characteristics, the period, halving time, and cycles to halve are determined. These are given in Table 15.

TABLE 15

short wing

	empty		gross	
	25 m/sec	100 m/sec	25 m/sec	100 m/sec
Dutch Roll				
T (sec)	0.73	0.18	1.1	0.15
t_{half} (sec)	0.72	0.16	3.24	0.47
N_{half}	0.99	0.86	2.94	3.12
Spiral Mode				
t_{half} (sec)	2.1	79.5	13.7	80
Rolling Mode				
t_{half} (sec)	0.05	0.013	0.12	0.03

long wing

	empty		gross	
	25 m/sec	100 m/sec	25 m/sec	100 m/sec
Dutch Roll				
T (sec)	0.727	0.199	33.5	0.55
t_{half} (sec)	0.857	0.17	1.0	0.313
N_{half}	1.18	0.85	33.5	1.74
Spiral Mode				
t_{half} (sec)	7.5	16.1	36	18
Rolling Mode				
t_{half} (sec)	0.02	0.005	0.05	0.013

From these figures it is seen that the aircraft is laterally stable in all modes with either wing at either speed.

These calculations confirmed the stability, both longitudinal and lateral, of the Glider - Mark II. The next step was construction.

VI. GLIDER - MARK II CONSTRUCTION

A) Wing

The wings were built using the foam core, fiberglass-epoxy skin technique. We didn't have foam cores already, as we had for the Glider - Mark I, so we had to cut our own. This was done by making aluminum templates of the modified NACA 65 - 418 wing section that we were using, fastening them to the ends of the uncut foam slab and then using a taut, hot nichrome wire to cut the foam, using the templates on either end as a guide. Since a balsa leading edge and aileron were to be added, the foam was cut sans leading edges and ailerons.

The leading edges were shaped from light balsa and epoxied to the foam cores. This was done since the hot wire cutter could not cut the sharp curve of the leading edge, but the balsa could easily be carved to the correct shape. Pine blocks were installed in the front and rear of the center section of both wing cores. These would later have holes drilled in them and be used to mount the wings on the fuselage. The short wing (AR 6) was then laid up with one layer of fiberglass-epoxy, the same as used on Glider - Mark I. The long wing (AR 12) was laid up with two layers of fiberglass-epoxy from the wing root to the half-span point and one layer from there outward to the tip. The orientation of the weave on both wings is shown in Figure 6.

For each wing a set of ailerons was made from hard balsa. Balsa wingtips were carved and epoxied to the tip of each wing. A cutout in the bottom of the center of each wing was made to hold the aileron servo in place. The wing was primered and painted with polyurethane paint, and then the aileron hinges were epoxied in place. A "Kavan" aileron hinge line fairing was used between the wing and the ailerons to reduce drag. The ailerons were then installed, along with their pushrods from the servo. This completed the construction of the two wings, shown in Figure 18.

FIGURE 18

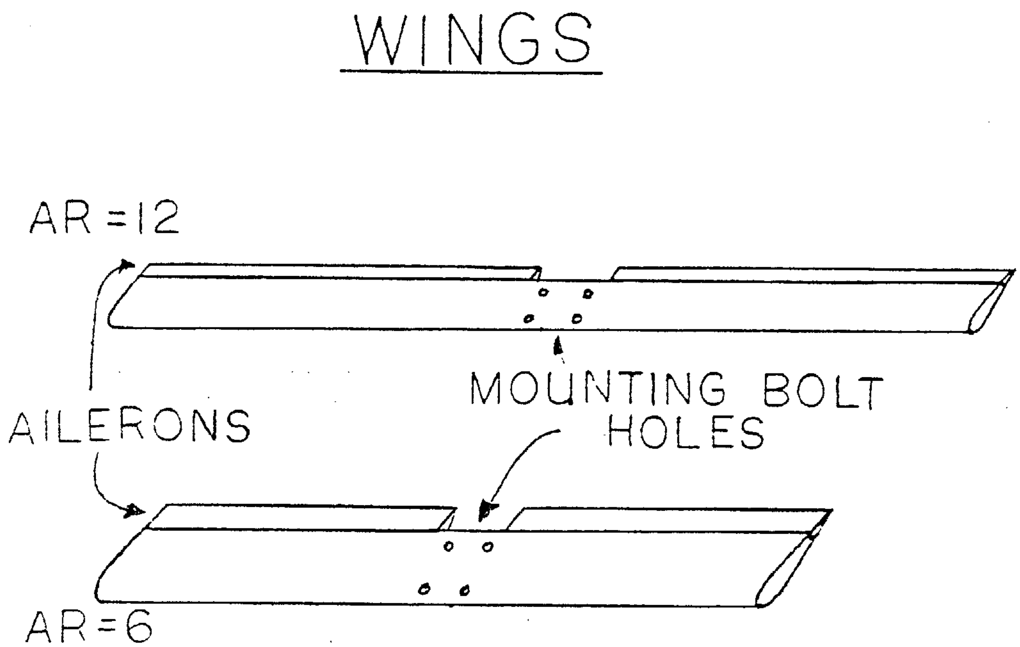

An adapter was made from plywood and balsa so that the long wing could fit in the short wing fuselage saddle so both wings could be installed in the same fuselage.

B) Fuselage

The fuselage frame was constructed from spruce stringers and plywood bulkheads. The two rear bulkheads (numbers three and four) were cut from three quarter inch plywood and the two front bulkheads (numbers one and two) were cut from three eigths inch plywood. The spruce stringers were one quarter inch square. These were cut to length and the frame was epoxied together. This framework is shown in Figure 19.

FIGURE 19

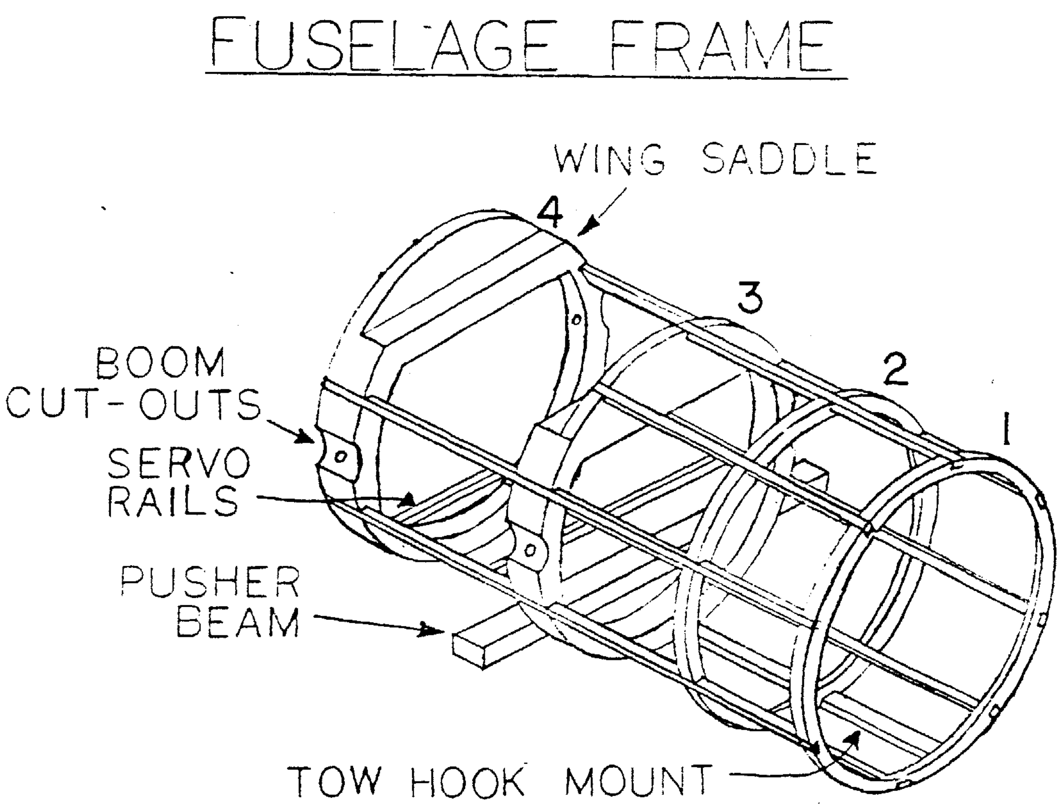

Next the 3/4" bulkheads had cutouts made for the tail-booms to nest in, and holes for the tail-boom mounting bolts were drilled. A wing nounting saddle was installed between them on top, along with wing hold-down bolt nuts. Servo mounting rails and electronics mounts (all made of

1/4" x 1/2" spruce rails) were epoxied in. The pusher beam was epoxied into place directly under the wing behind bulkhead three, above stringers numbers five and six. The pusher beam was 1/2" x 1" spruce laminated with two pieces of 1/16" G-10 (fiberglass-epoxy composite) top and bottom. A piece of spruce was epoxied on the bottom of the frame between bulkheads one and two, and two and three. This would later be used as a towhook and skid support. All these can be seen in Figure 19 above. This completed the major fuselage structure.

Next came the fuselage covering. The first step was to epoxy a skin of 1/16" light balsa completely over the fuselage except for the wing and tail boom mounting areas. One layer of fiberglass-epoxy was then laid up over the balsa except on the bottom, where two layers were used for abrasion protection during landings. The tow hook and landing skid were then installed.

The nose and tail cones were carved from foam and covered with one layer of fiberglass-epoxy which overhung the foam one centimeter in the rear. This overhang fitted around the fuselage, and two screws were screwed through it to secure each of the cones to the fuselage.

TAIL and BOOMS

An exploded view of the tail and booms is seen in Figure 20.

FIGURE 20

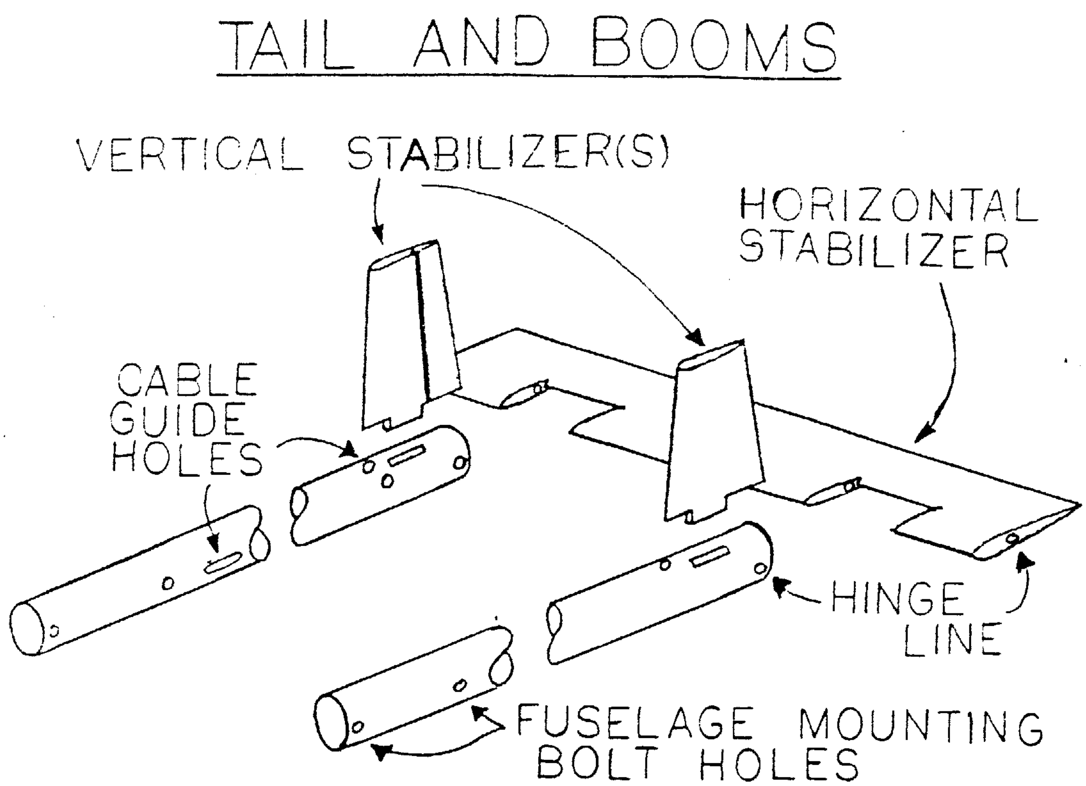

The horizontal and vertical tail components were carved from light balsa and covered with one layer of fiberglass-epoxy. Only one of the vertical stabilizers had a rudder. This simplified construction and control linkages. The horizontal stabilizer was an all moving type, pivoting on a music wire in a brass tube hinge. This simplified construction and the control linkages also, but more importantly increased the stabilizer effectiveness.

The tail booms were lengths of 1.25" diameter 1/32" wall thickness aluminum tubing. These had pine plugs epoxied inside them in three places; the two tube-fuselage mounting points and the horizontal stabilizer hinge line. These supported the tube at concentrated stress areas. Holes were then drilled for the mounting bolts, stabilizer hinge, vertical stabilizer mounting lugs, and tail skid mounting lugs. The fiberglass-epoxy covered tail skids were epoxied to the bottom of each boom, and a vertical stabilizer was epoxied to the top of each boom. Holes were then drilled in the booms for the control cable guides to pass through. The braided steel control cables and their guides were installed and then the booms were attached to the horizontal stabilizer by sliding the music wire hinge through the stabilizer, one boom, the stabilizer center section, the other boom, and then the final secton of the stabilizer. Two screw collars kept the music wire in place. This completed the tail and boom assembly.

A view of the completely assembled Glider - Mark II is seen in Figure 21.

FIGURE 21

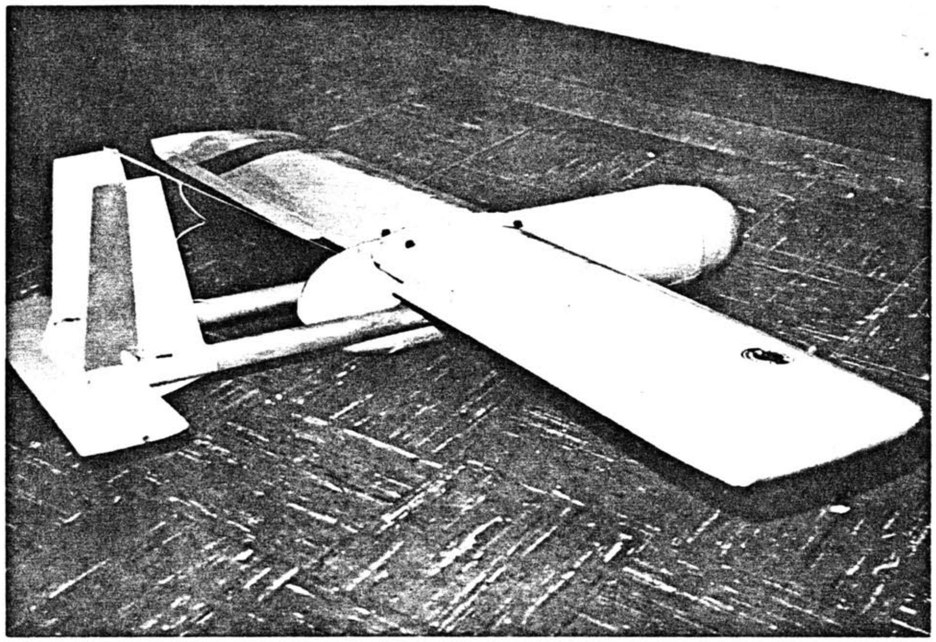

D) Control System

The control system included the battery pack, receiver, antenna, three heavy duty servos, and all the control linkages. The rudder and horizontal stabilizer servos were installed on the servo mounting rails directly under the wing by screwing them down. The braided steel control cables (two for each servo) entered their guides inside the rear of the fuselage and then went inside the tail booms. The rudder cables were inside the left boom and the horizontal stabilizer cables were inside the right boom (as seen from the front). At the rear of the booms the cables exited and were connected to control horns on either side of each control surface (rudder and horizontal stabilizer).

An aileron servo was mounted in the bottom of the center of each wing, and connected to each aileron by bent music wire rods.

The battery pack and receiver were wrapped in foam rubber and installed in the front of the fuselage between bulkheads one and three and the electronics mounts. The antenna exited the fuselage by the front cone and was fastened to the fuselage with silicone RTV. It ran back under the wing and then up to the top of the vertical stabilizer.

E) Yoke

The yoke for the Glider - Mark II was an aluminum frame that bolted to the front and rear of the bucket. A schematic is shown in Figure 22.

FIGURE 22

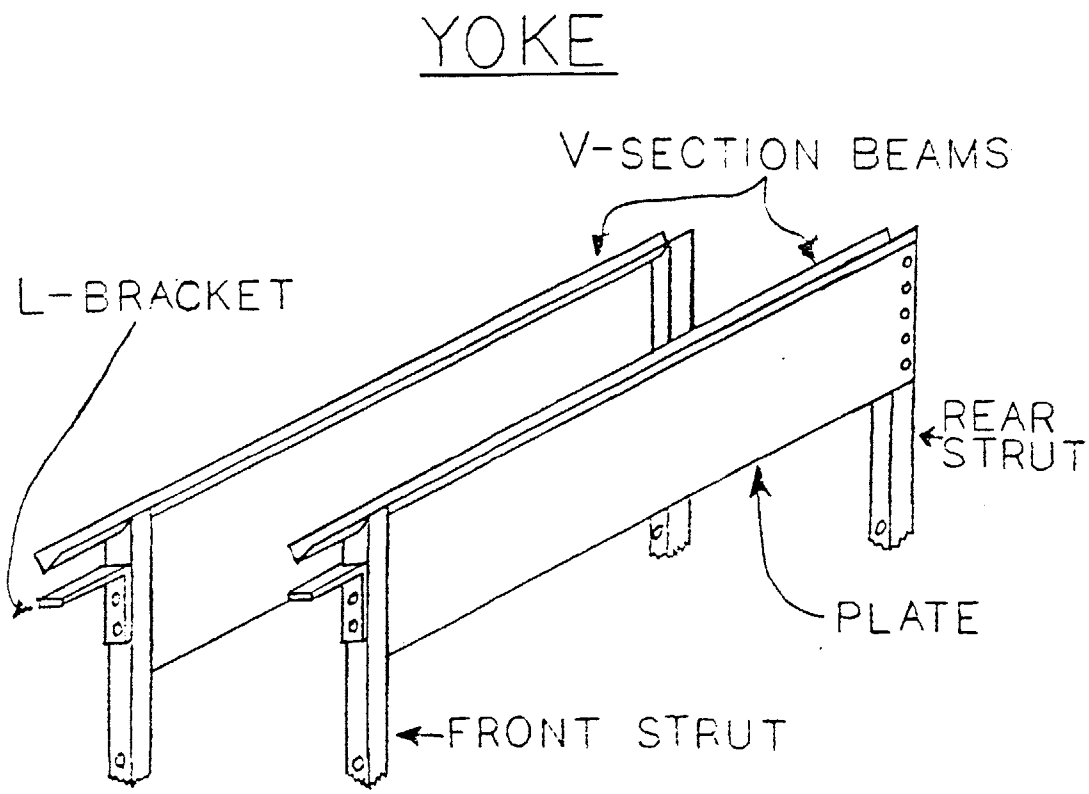

There were four identical aluminum struts that were bolted to the bucket via the bucket's threaded rods. A 1/8" wall thickness V-section aluminum beam was welded to the top of the front struts. A 1/8" thick aluminum plate four inches wide was welded to the side of each front strut and to the side of each V-section beam. Each plate was then screwed into one drilled and tapped rear strut to hold the whole system together. An L-bracket was screwed into the front of each front strut as part of the glider pusher-beam constraints.

The glider rested on the yoke with the pusher-beam held by the L-brackets and the V-sections. The tail boom skids rested in the top of the V-sections. As the bucket accelerated, the front struts pushed on the pusher-beam, while the down load on the booms was transferred to the rear struts via the V-sections. The front V-sections and L-brackets transferred any up or down loads on the front of the glider to the front struts. When the bucket decelerated, the glider slid out of the yoke, while the V-sections guided the booms, keeping them and the tail clear of any obstructions or the front of the yoke.

VII. FLIGHT TESTING

A) Conventional Launches

The same procedure was used for flight testing the Glider - Mark II as was used for the Glider - Mark I. When the construction was completed in July 1981, the glider was assembled. The ailerons, rudder, and elevator were then trimmed by eye. Adrian Nye, Osa Fitch, Whitney Hamnett and I took the aircraft, radio control set, and Hi-Start launcher out onto Briggs field. Because of the weight of the aircraft and its high stall speed (~25 mph) a hand launch was impossible, since no-one could throw it that fast. A Hi-Start launch was therefore attempted. The plane accelerated slowly and then began to climb, reaching an altitude of 50 meters before it released from the Hi-Start. Adrian flew a left turn, straightened out and then turned into the wind for a smooth landing. Because of the slow acceleration and low altitude gain, we decided to procure another Hi-Start and use two of them in parallel for any subsequent launches.

With the dual Hi-Start, the launchings became much smoother and quicker, with somewhat more altitude gain. It was determined that the ailerons were too sensitive to control movements and the roll control was poor. The sensitivity was reduced, and the later flights were very satisfactory. A few hard landings attested to the strength of the fuselage and the tail, with even an upside down landing causing no damage. Adrian was able to set up all the trim settings for the three controls, and then the aircraft was deemed ready for an electromagnetic launch.

B) Electromagnetic Launches

No electromagnetic launches have been attempted yet, because of minor problems with the launcher. However, the glider and yoke assembly are complete and have been fitted to the launcher bucket. An electromagnetic launch is expected within two weeks.

VIII. CONCLUSIONS and RECOMMENDATIONS

A) Conclusions

From the work done with the Glider - Mark I, the main conclusion that can be reached is that it is possible to launch an aircraft from an electromagnetic launcher at high accelerations. It is possible to launch a small, cheap glider at up to 100 gees and six times its glide velocity while having complete control over it the whole time. There do not seem to be any basic difficulties with the process although a full launch to 80 m/sec has not been accomplished yet. I believe that if an aircraft is built to withstand the rigors of a 100 gee launch along with a very high launch velocity, there are no strange interactions or transients that occur in the very short launch interval which would inhibit normal flight.

It seems as though a glider for electromagnetic launching purposes can be built to have a payload ratio of at least 50% with the simple construction methods and conservative design principles used in this report. It is my belief that this ratio could be raised to ~75% (along with a higher glide ratio) by using less conservative design principles, lower safety factors, and by going to more advanced materials and construction processes.

B) Recommendations

Of course, my first recommendation is that electromagnetic launches with the Glider - Mark II be tried, both with the short wing and the long wing, at velocities up to 80 m/sec. Next, I believe that a full scale Cargo Glider should be built along with a full scale launcher for it. From there, work can be done to increase the performance (glide ratio) while maintaining stability, and decrease the empty weight (increase the payload ratio). These may be done by using Kevlar and graphite composites for a great deal of the structure, allowing longer wings and lighter components.

There are other configurations af the aircraft that have not been examined here because of time constraints. Some of these are: a canard, a folding wing for launch, a folding wing canard, and an inflatable wing which inflates after launch. It may be that higher glide distances may be achieved and higher payloads may be carried with these configurations. I believe that there is much work left to do in these areas.

IX. APPENDICES

A) Michael Paluszek's Trajectory Analysis

TRAJECTORY ANALYSIS for an
ELECTROMAGNETICALLY LAUNCHED
GLIDER

by

Michael A. Paluszek

M.I.T.

April 1980

1. Introduction

The purpose of this phase of the program was to determine the vehicle and launch configuration that would produce the maximum range for a given initial velocity at the exit of the electromagnetic accelerator. The glider characteristics available for modification were the wing aspect ratio (AR) and the wing loading. Given the launch velocity, the only launch parameter that could be varied was the launch angle, although the glider angle of attack was assumed to be controllable (if desired) during flight.

The limits for allowable aspect ratios and wing loadings were calculated by the glider design group, as were all the other vehicle parameters. Maximum launch weight and velocity were given by the accelerator group. Table 1.1 summarizes the relevant information.

Parameter	Value (or range)
C_{D_p}	.03
m	23kg
C_{ℓ_α}	2π
e	.95
s	$.2m^2 \rightarrow .65m^2$
AR	6 to 13
V_i	88m/sec

Table 1.1 Glider Data

The basic procedure was to numerically integrate the equations of motion to obtain the flight path, and maximum range, varying AR, γi and m/s in a heuristic fashion until the maximum range was achieved. No attempt was made to formally optimize the glider.

Since the philosophy was to design as simple a glider as possible the emphasis was on simple vehicle controls, unless a large gain in range, commensurate with the increase in complexity, could be obtained. The cases studied were the fixed angle of attack case and the ballistic launch case, where the wing produces lift only once the trajectory peak is reached.

This report is divided into three parts detailing the equation of motion, the numerical techniques and the results respectively. Copies of the computer code are included as an appendix.

2. The Equations of Motion

The equations of the motion were written in the flight path axis, as illustrated in Figure 2.1, by the balancing of forces. The equations are:

$$m \frac{du}{dt} = -D - mg \sin \gamma$$

$$mv \frac{d\gamma}{dt} = L - mg \cos \gamma \tag{2.1}$$

where γ is the angle to the horizontal, m is the glider mass, v its velocity, g the acceleration of gravity, D the total drag and L the total lift.

The drag is defined by the equation

$$D = \frac{1}{2} \rho v^2 A \, C_D \tag{2.2}$$

where ρ is the air density, C_D the drag coefficient and A is the drag reference area. The lift is similarly defined as

$$L = \frac{1}{2} \rho v^2 \, S \, C_L \tag{2.3}$$

where S is the lifting surface area and C_L is the lift coefficient.

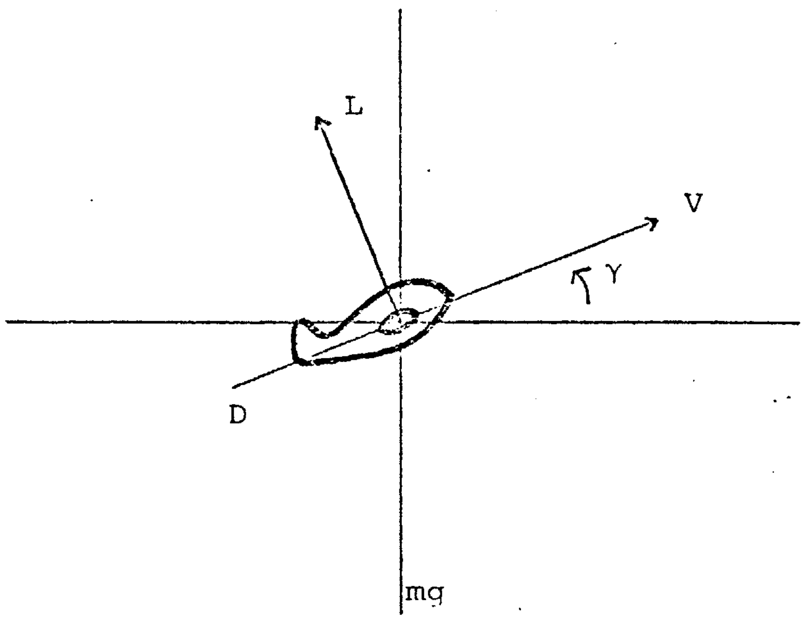

2.1 Flight Path Axis

The drag coefficient is composed of two elements, one is the lift independent drag and the other the drag induced due to lift.

$$C_D = C_{D_p} + \frac{C_L^{\,2}}{\pi e AR} \tag{2.4}$$

The lift coefficient is derived from thin airfoil theory[4] and is

$$C_L = \frac{C_{L\gamma}}{1 + \frac{C_{L\gamma}}{\pi AR}} \alpha \tag{2.5}$$

$$C_{L\alpha} = 2\pi$$

The air density is assumed to be an exponential function of altitude and is given by

$$\rho = 1.2\ e^{-h/6341} \tag{2.6}$$

with ρ in kg/m^3

3. Numerical Methods

A fourth order Runge-Kutta method was used to integrate the equations numerically. The four equations of motion are arranged as follows

$$\frac{du}{dt} = -D/_m - g \sin \gamma$$

$$\frac{d\gamma}{dt} = \frac{L}{mv} - g/_v \cos \gamma$$

$$\frac{dv}{dt} = v \cos \gamma \qquad (3.1)$$

$$\frac{dv}{dt} = v \sin \gamma$$

The right hand sides are functions of V, γ and y.

The algorithm used is an extension of the two first order equation case as given in Hildebrandt.[2] The error is on the order of $(\Delta t)^4$. For the trajectory analysis $\Delta t = 1$ sec and the algorithm was implemented on a PDP 11/10 using single precision arithmetic.

4. Results and Conclusions

4.1 Introduction

In order to establish a baseline vehicle a wide variety of vehicle configurations were simulated on the computer. The cases can be grouped into three general types; ballistic, fixed angle of attack and variable angle of attack. Maximum ranges and optimum launch angles were calculated for all the cases and the results used to choose a configuration for actual construction.

4.2 The Ballistic Vehicles

The simplest case was the ballistic projectile with no lifting surfaces. With a drag coefficient of $C_{D_p} = .03$ and a launch angle of 45^{o} the range was 644m. With $C_{D_p} = .001$ this range increased to 804 m. Essentially, this is an artillery shell with no controls and the simplest structure, due to the absence of wings.

4.3 The Constant Angle of Attack

The constant angle of attack configuration was the next simplest design with the wing preset at a given angle of attack and no active controls. The improvement in range over the ballistic case (with equal C_{D_p}) was 113 m for an aspect ratio of 6 and 192.4 m for an aspect ratio of 13. The reason for this relatively poor performance is the need to maintain stable flight over a wide velocity range and during the very steep climb. Unless the angle of attack at launch is kept well below the angle for optimum L/D the glider will loop. Besides the short range, this configuration has very high landing velocities unless provisions are made for a flare at landing.

4.4 The Variable Angle of Attack

Since it is difficult to obtain good range in a vehicle designed for a high velocity boost and for gliding, the obvious step was to separate the two flight conditions and optimize for each with some simple control system providing the transition. The result was a combination of the previous two cases with a ballistic launch and lifting glide. The wings are deployed on launch but are set to provide no lift. At the peak of the trajectory an actuator sets the wings at the angle of attack for maximum L/D as determined by the relationship.

$$\alpha_{max\ L/D} = \sqrt{\frac{\pi e AR\ C_{D_p}}{C_{\ell_\alpha}^{2}}} \tag{4.4.1}$$

If the air density does not vary significantly this will produce the maximum glide distance. The glide distance for the constant angle of attack is[3]

$$\Delta\chi = \frac{C_L}{C_D}\left(h_i - h_f + \frac{V_i^2 - V_f^2}{2g}\right) \tag{4.4.2}$$

where h is the altitude and v the velocity. Since ρ varies less than 5% in all the analyzed trajectories, this relationship is good for the cases of interest.

The free parameters for this analysis were taken to be γ_i, the launch angle, AR and s, the wing surface area. γ_i determines the peak height of the trajectory and the cross-range during the ballistic flight while the latter two, along with the trajectory peak, determine the gliding range.

The procedure was to find an optimum combination of γi and s for every given AR, then to compare the optimums at each AR with each other.

Figures 4.1 and 4.2 give maximum ranges vs. wingloading for AR = 6 and 13, respectively. Each maximum is achieved at a given optimum launch angle which is given in figures 4.3 and 4.4. For each AR there is a wingloading that gives maximum total crossrange. The peak range is achieved with wingloadings on the order of 9.5 to 10 lbs/ft^2. The roll off in range after the peak is due to the increase in drag during ballistic flight which reduces the trajectory peak and the ballistic crossrange.

Figure 4.5 gives the maximum ranges versus AR for AR ranging from 6 to 20. The variation with AR is nearly linear. Theory predicts that for gliding flight at optimum L/D the range should vary as $\sqrt{AR}$. This proves to be the case when the ballistic crossrange is subtracted from the total range and the increase in peak trajectory height is accounted for.

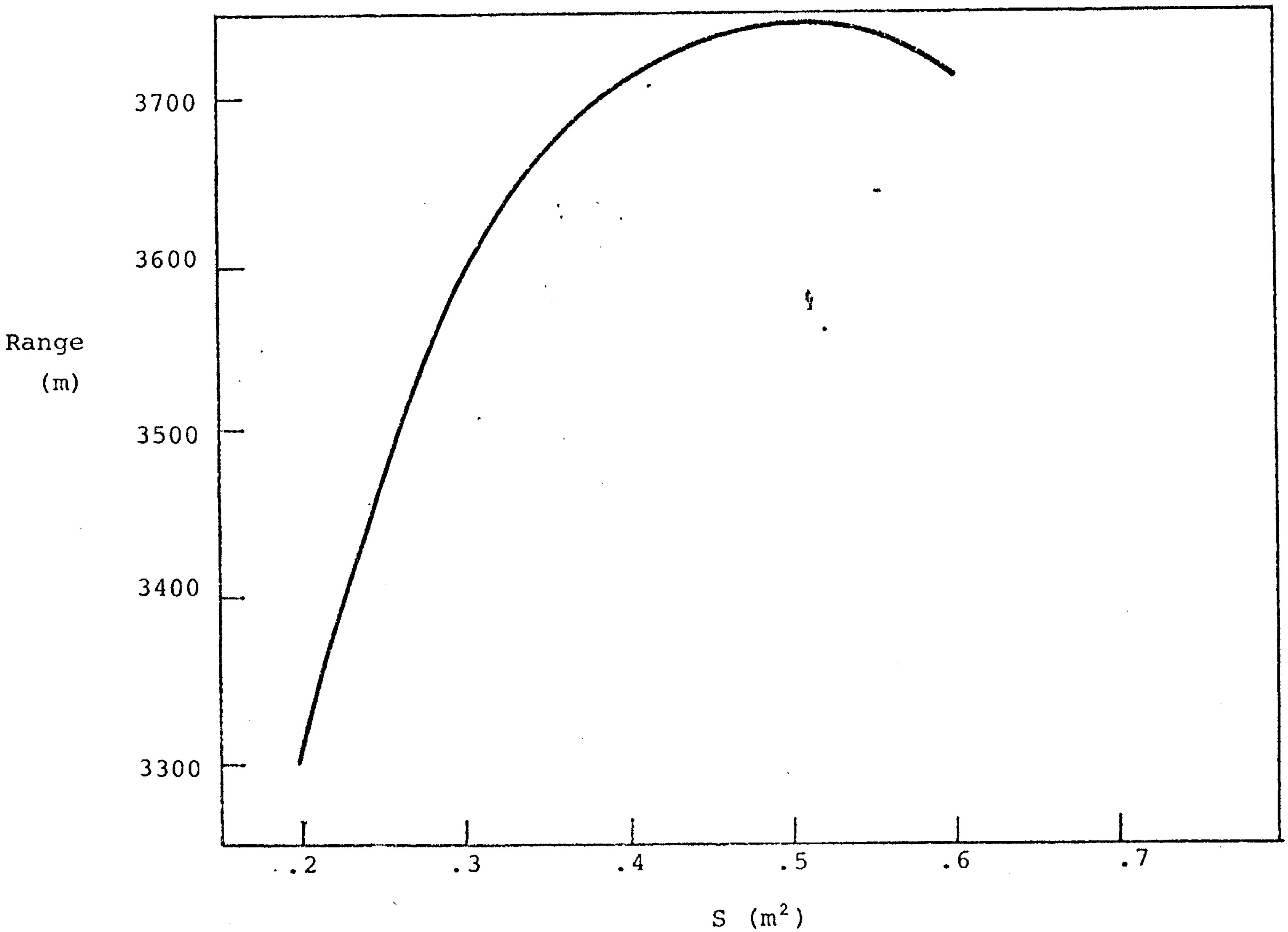

Figure 4.1 Maximum Range vs. Wingloading
AR = 6

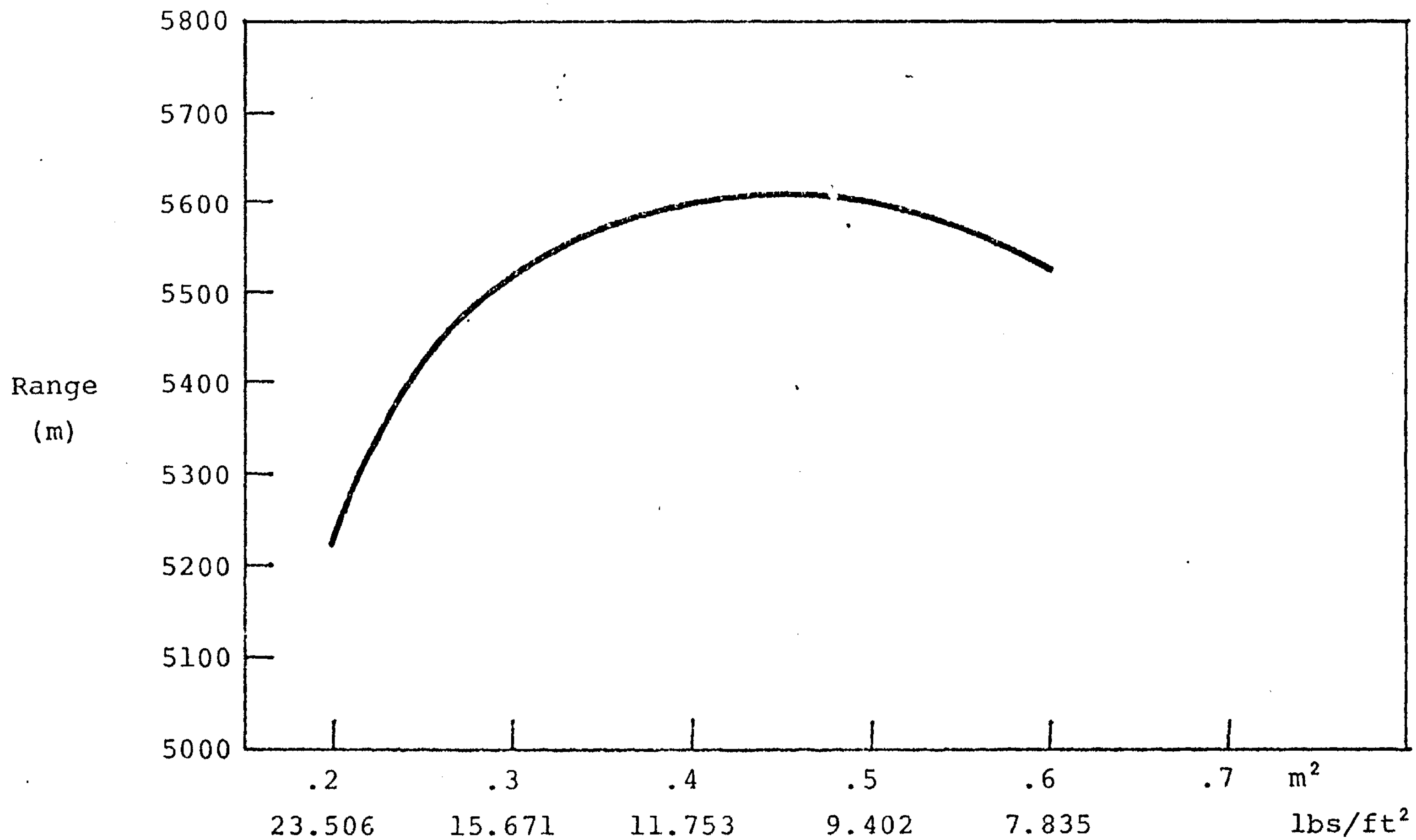

Figure 4.2 Maximum Range vs. Wingloading for Ballistic Launch

AR = 13

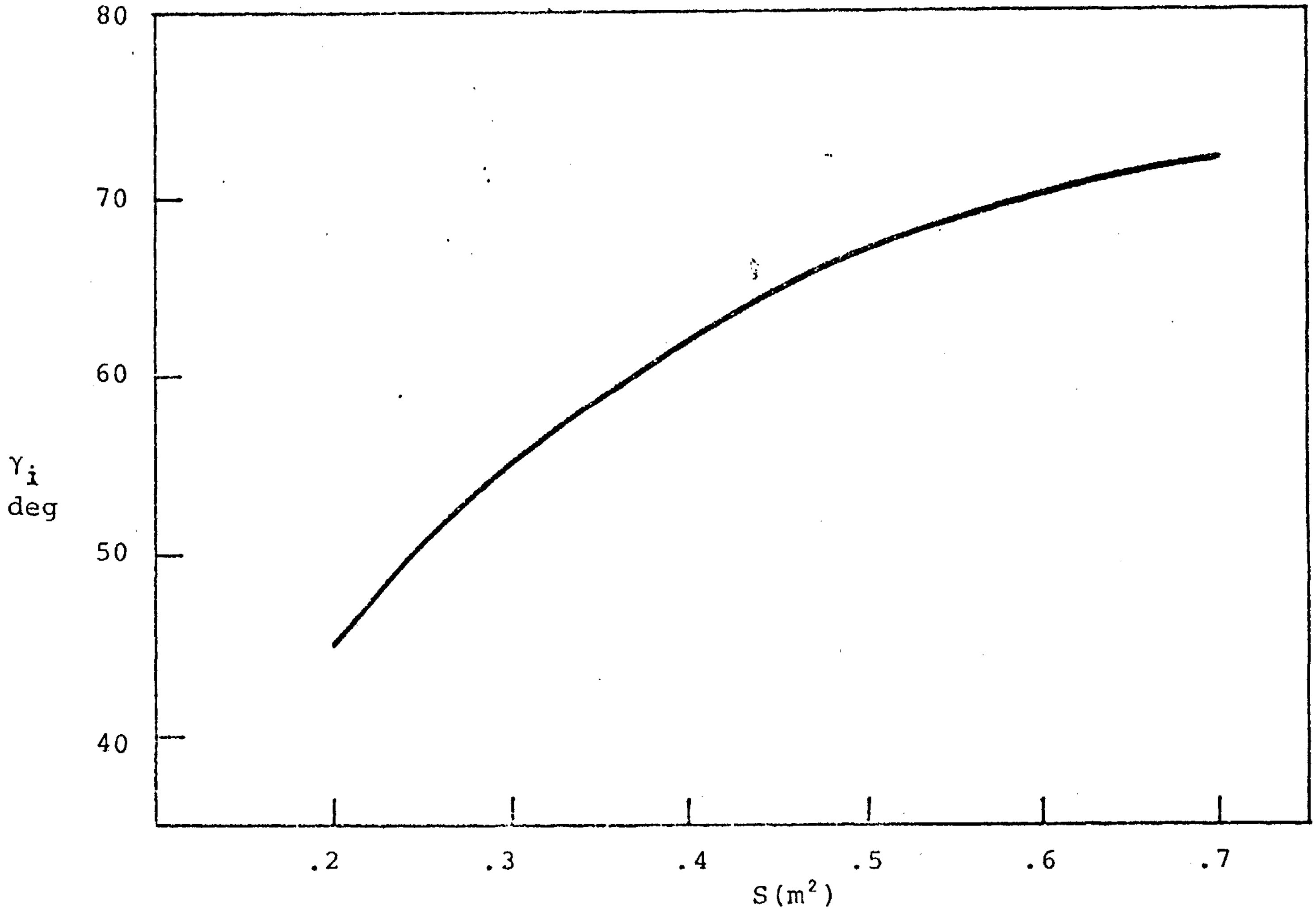

Figure 4.3 Optimum launch angle vs. wing area

$\text{AR} = 6$

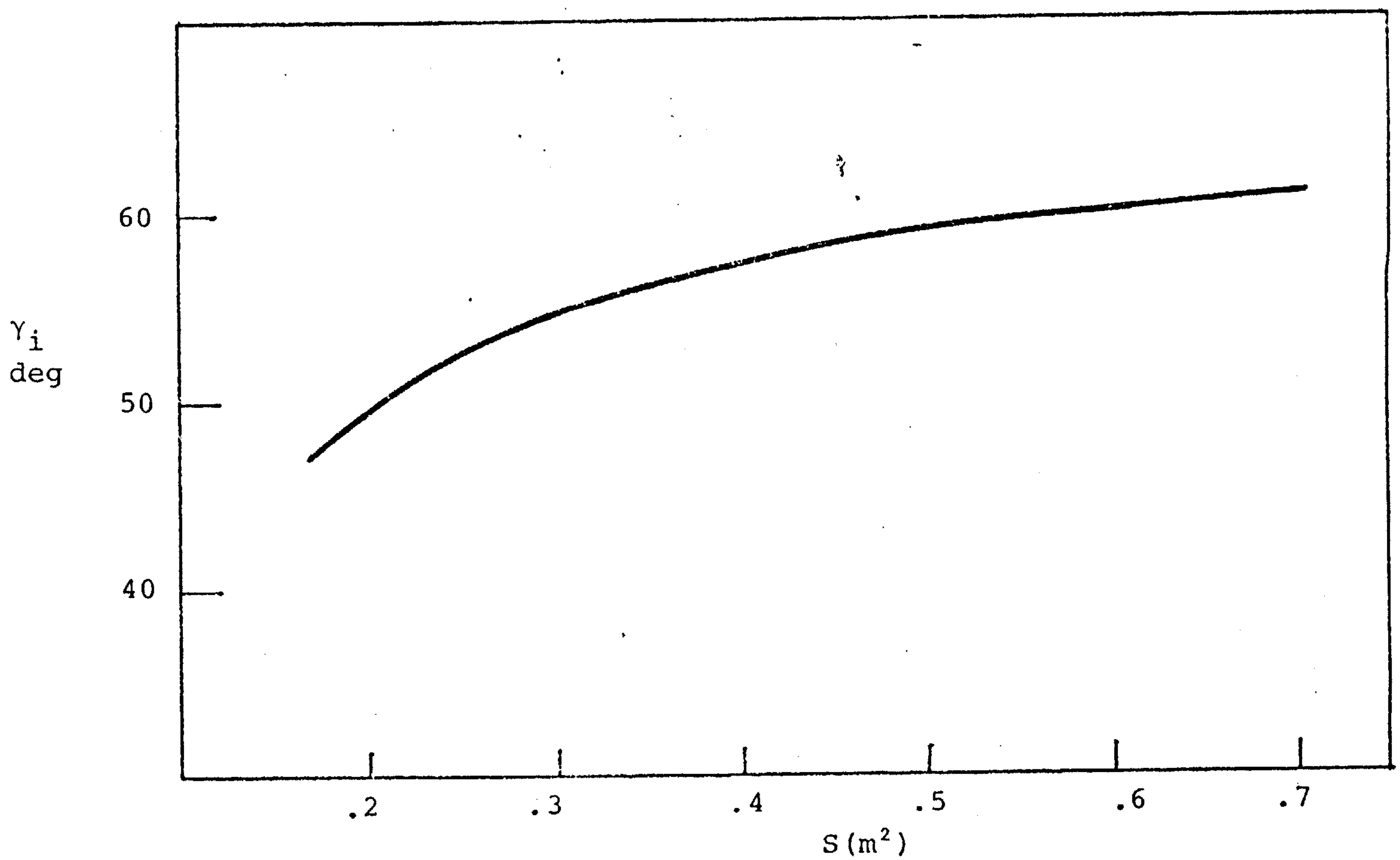

Figure 4.4 Optimum launch angle vs. wing area

$AR = 13$

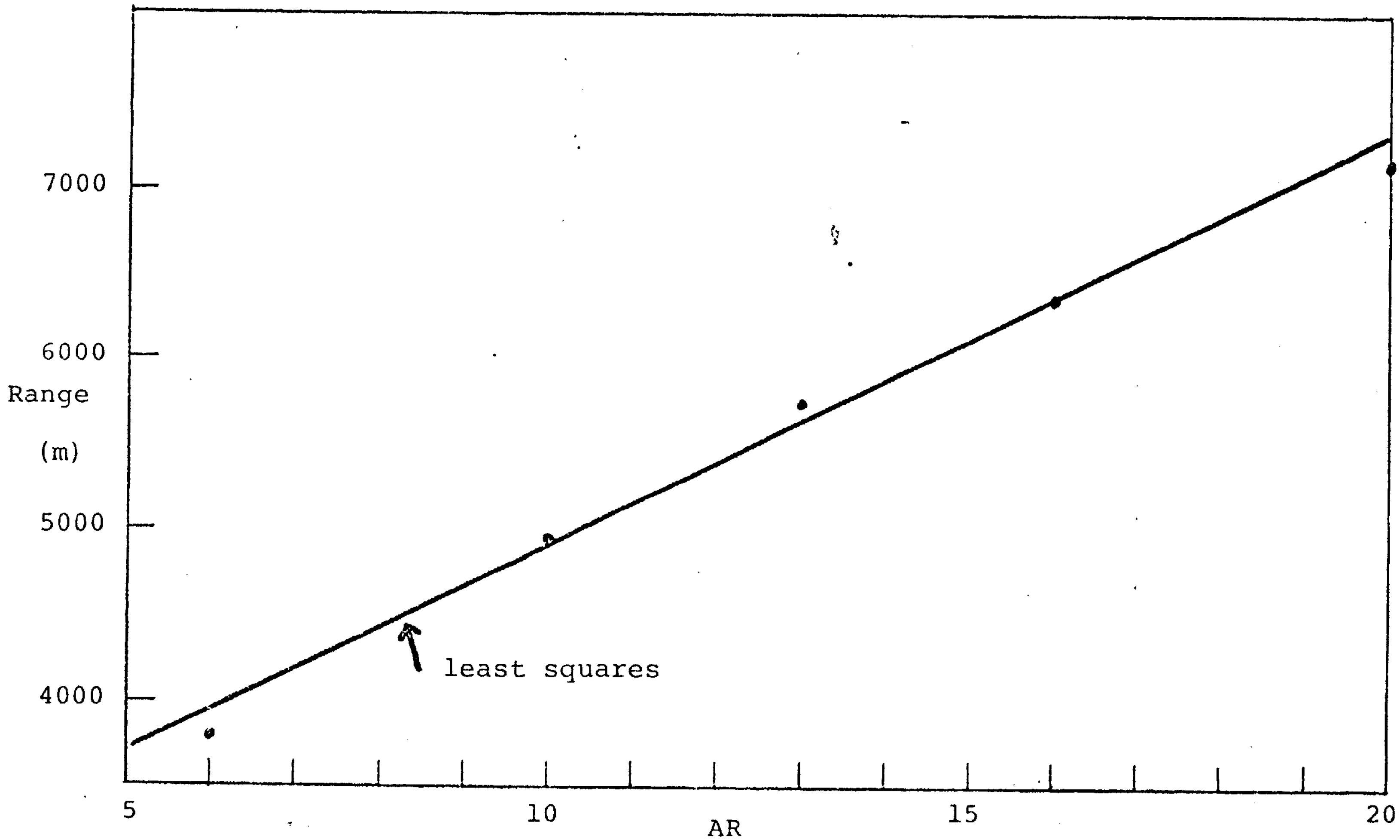

Fig. 4.5 Maximum range vs. AR

4.6 Conclusions

Table 4.1 gives a summary of the data for all the cases examined. Figure 4.6 shows representative trajectories for the ballistic, constant angle of attack and variable angle of attack cases.

The best configuration is the variable angle of attack design with as large as aspect ratio as possible. The only limit to aspect ratio would be due to structural considerations. The wing loading should lie between 9.5 and 10 lbs/ft^2 and launch angles will be in excess of 70°. Any limits due to diminishing returns on AR will only occur for very large AR when the AR law begins to reassert itself as γ_i reaches a limit. A further limit may be that the high angles of attack needed for optimum L/D at large AR may be difficult to realize.

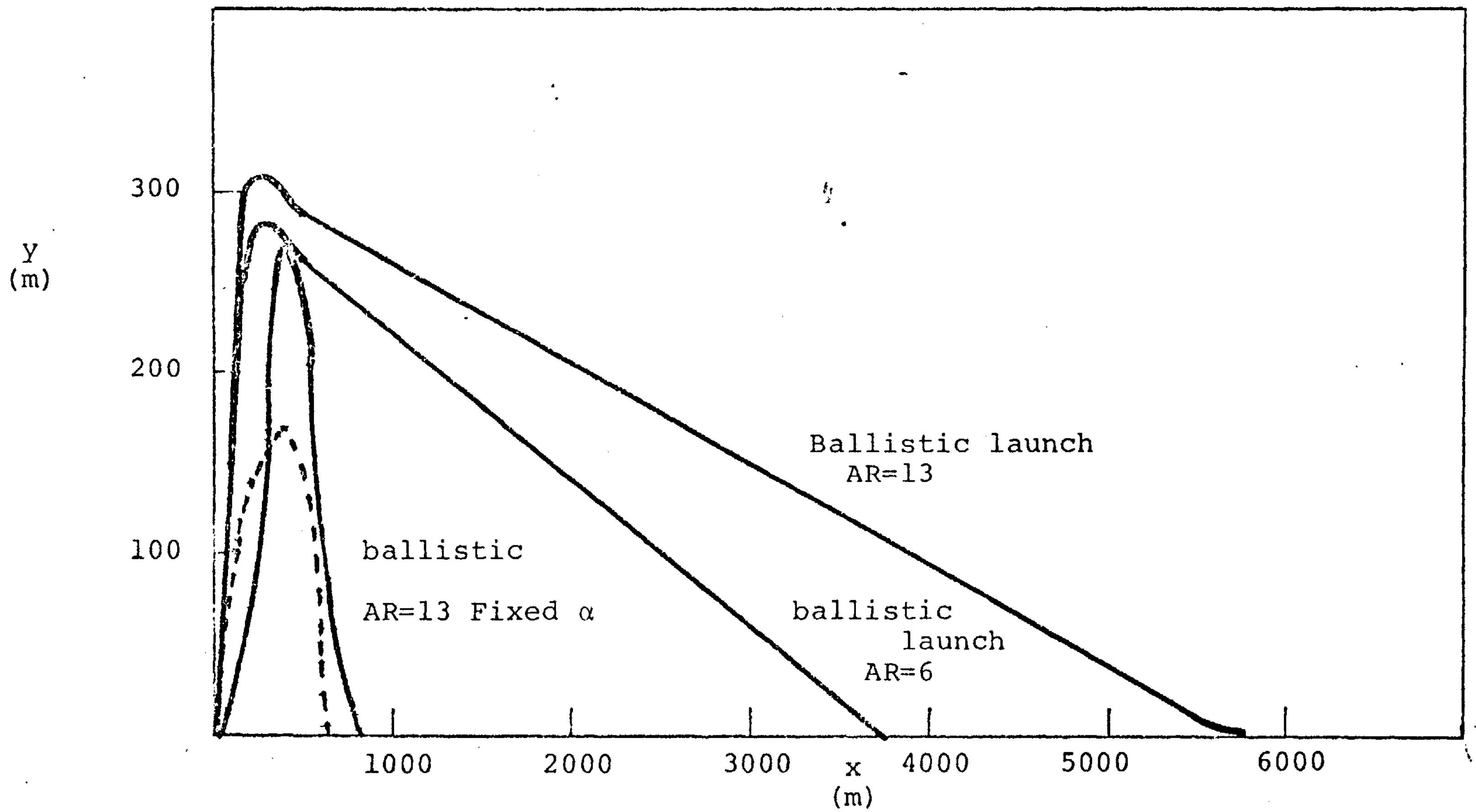

Figure 4.6 Trajectories for Ballistic with $C_{D_p} = .03$, Fixed α AR-13; Ballistic Launch: AR = 6; AR = 13

Table 4.1   Summary of Results

Case	γ_i	S	α	max range
	Deg	m^2	Deg	m
ballistic (C_{D_p} = .001)	45	0	0	808
ballistic (C_{D_p} = .03)	45	0	0	644
fixed α				
AR = 6	0	.2	8.9	757
AR 13	0	.3	5	836
variable α, ballistic launch				
AR = 6	65	.50	8.9	3744
10	70	.45	10.5	4940
13	70	.45	11.4	5715
16	70	.50	12.3	6362
20	70	.50	13.4	7155

References

1. Larrabee, E.E., _Flying by Computer_, 16.15 course notes, MIT, Spring 1978.

2. Hildebrandt, F.B., _Introduction to Numerical Analysis_, McGraw-Hill, NY 1956, p.237.

3. Miele, A., _Flight Mechanics_, 1962 Addison-Wesley, Reading, MA.

4. Kuethe, A.M., and Chow, C., _Foundations of Aerodynamics_, Wiley, NY. 1976, p. 155.

APPENDIX: The Computer Program

```
 TYPE DL0:TRJ.FOR
C   THIS PROGRAM USES THE RUNGE KUTTA INTEGRATION
C   TECHNIQUE TO SOLVE THE LONGITUDINAL EQUATIONS
C   OF MOTION FOR AN ELECTROMAGNETICALLY LAUNCHED
C   GLIDER
        REAL L,M,LOVERD
        COMMON/AEROPR/CDP,CLALPH,S,AR,E,A,M,ALPHA,AUNDER
10      FORMAT(40H INPUT CDP,CLALPHA,AR,E,M FOR THE GLIDER)
11      FORMAT(40H CDP IS THE LIFT INDEPENDENT DRAG COEFF.
        1/26H CLALPH IS THE LIFT COEFF.
        2/22H S IS THE SURFACE AREA
        3/28H AR IS THE WING ASPECT RATIO
        4/19H E IS THE AERO. EFF
        5/14H M IS THE MASS
        6/22H A IS THE FRONTAL AREA)
        TYPE 11
        TYPE 10
        PI=3.14159
16      FORMAT(5F12.4)
15      FORMAT(4F12.4)
        READ(5,16) CDP,CLALPH,AR,E,M
        CLALPH=CLALPH/(1.+CLALPH/(PI*AR))
20      FORMAT(26H INPUT DT IN SECS,Y0,X0,V0)
        TYPE 20
        READ(5,15) DT,YI,XI,VI
151     FORMAT(23H INPUT DEPLOYMENT GAMMA)
        TYPE 151
        READ(5,118) GAMMAD
        GO TO 150
147     FORMAT(29H INPUT ANGLE OF ATTACK IN DEG)
150     TYPE 147
        READ(5,118) ALPHIN
        ALPHIN=ALPHIN*3.14159/180.
        IF(ALPHIN .GE. 0.) GO TO 167
        ALPHIN=SQRT(PI*E*AR*CDP/CLALPH**2.)
        IF(ALPHIN .GT. .2792) ALPHIN=.2792
118     FORMAT(F12.4)
155     FORMAT(17H ANGLE OF ATTACK=,F8.3,5H DEG.)
        TYPE 155, ALPHIN*180./PI
160     FORMAT(6F12.4)
157     FORMAT(52H INPUT LIMITS,SI,SF,DELTAS,GAMMAI
        1,GAMMAF,DELTA GAMMA)
167     TYPE 157
        READ(5,160) SI,SF,DELS,GI,GF,DELG
        GI=PI*GI/180.
        GF=PI*GF/180.
```

```
      DELG=PI*DELG/180.
      S=SI-DELS
175   S=S+DELS
      A=S
      GAMI=GI-DELG
      IF(S .GT. SF+DELS/2.) GO TO 1000
170   FORMAT(15H WING LOADING =,F8.3,8H LBS/FT2)
      TYPE 170,M/S*.2044
185   GAMI=GAMI+DELG
      IF(GAMI .GT. GF+DELG/2.) GO TO 175
      X=XI
      Y=YI
      V=VI
      GAM=GAMI
      IA=0
C  THESE ARE THE RUNGE KUTTA SUBROUTINE CALLS
C  X IS THE HORIZONTAL DISTANCE, Y THE ALTITUDE
C  AND GAM IS GAMMA THE FLIGHT PATH ANGLE
200   ALPHA=ANGLE(Y,GAM,ALPHIN,IA,GAMMAD)
210   V0=DT*F1(Y,V,GAM)
      GAM0=DT*F2(Y,V,GAM)
      X0=DT*F3(Y,V,GAM)
      Y0=DT*F4(Y,V,GAM)
      V1=DT*F1(Y+.5*Y0,V+.5*V0,GAM+.5*GAM0)
      GAM1=DT*F2(Y+.5*Y0,V+.5*V0,GAM+.5*GAM0)
      X1=DT*F3(Y+.5*Y0,V+.5*V0,GAM+.5*GAM0)
      Y1=DT*F4(Y+.5*Y0,V+.5*V0,GAM+.5*GAM0)
      V2=DT*F1(Y+.5*Y1,V+.5*V1,GAM+.5*GAM1)
      GAM2=DT*F2(Y+.5*Y1,V+.5*V1,GAM+.5*GAM1)
      X2=DT*F3(Y+.5*Y1,V+.5*V1,GAM+.5*GAM1)
      Y2=DT*F4(Y+.5*Y1,V+.5*V1,GAM+.5*GAM1)
      V3=DT*F1(Y+Y2,V+V2,GAM+GAM2)
      GAM3=DT*F2(Y+Y2,V+V2,GAM+GAM2)
      X3=DT*F3(Y+Y2,V+V2,GAM+GAM2)
      Y3=DT*F4(Y+Y2,V+V2,GAM+GAM2)
      V=V+1./6.*(V0+2.*V1+2.*V2+V3)
      GAM=GAM+1./6.*(GAM0+2.*GAM1+2.*GAM2+GAM3)
      X=X+1./6.*(X0+2.*X1+2.*X2+X3)
      Y=Y+1./6.*(Y0+2.*Y1+2.*Y2+Y3)
      IF(Y .GT. 0.1 .AND. V .GT. 1.) GO TO 200
      LOVERD=WLIFT(Y,V,S,CLALPH,ALPHA)/
      1DRAG(Y,V,CDP,CLALPH,A,ALPHA,AR,E,0.)
      TYPE 555,GAMI*180./PI,S,X,LOVERD,V,V*SIN(GAM)
555   FORMAT(15H GAMMA INITIAL=,F4.0,11H WING AREA
```

```
      1=,F6.2,3H X=,F6.1,5H L/D=,F6.2,3H V=,F6.1,4H VY=,F6.1)
      GO TO 185
1000  END
C   THESE ARE THE RIGHT SIDES OF THE DN/DX=
C   FOR N: V,GAM,X,Y
      FUNCTION F1(Y,V,GAM)
      REAL M
      COMMON/AEROPR/CDP,CLALPH,S,AR,E,A,M,ALPHA,AUNDER
      G=9.8
      D=DRAG(Y,V,CDP,CLALPH,A,ALPHA,AR,E,AUNDER)
      F1=-D/M-G*SIN(GAM)
      RETURN
      END
      FUNCTION F2(Y,V,GAM)
      REAL M,L
      COMMON/AEROPR/CDP,CLALPH,S,AR,E,A,M,ALPHA,AUNDER
      G=9.8
      L=WLIFT(Y,V,S,CLALPH,ALPHA)
      F2=L/M/V-G/V*COS(GAM)
      RETURN
      END
      FUNCTION F3(Y,V,GAM)
      F3=V*COS(GAM)
      RETURN
      END
      FUNCTION F4(Y,V,GAM)
      F4=V*SIN(GAM)
      RETURN
      END
C   THIS FUNCTION COMPUTES THE DRAG
      FUNCTION DRAG(Y,V,CDP,CLALPH,A,ALPHA,AR,E,AUNDER)
      RHO=DENS(Y)
      CD=CDP+CL(ALPHA,CLALPH,V,Y)**2/3.14159/E/AR
      DRAG=.5*RHO*V**2.*A*CD
      RETURN
      END
C   THIS FUNCTION COMPUTES THE LIFT
      FUNCTION WLIFT(Y,V,S,CLALPH,ALPHA)
      RHO=DENS(Y)
      WLIFT=.5*RHO*V**2.*S*CL(ALPHA,CLALPH,V,Y)
      RETURN
      END
```

```
      FUNCTION DENS(ALT)
      DENS=1.2*EXP(-ALT/6341.)
      IF(ALT .LT. .01) DENS=1.2
      RETURN
      END
C  THIS FUNCTION COMPUTES THE LIFT COEFFICENT
      FUNCTION CL(ALPHA,CLALPH,V,Y)
      REAL MACH
      RHO=DENS(Y)
      A=291.102*SQRT(RHO)
      MACH=V/A
      IF(MACH .LT. .98 .AND. MACH .GE. 0.) GO TO 20
      TYPE 15,V,A,MACH
15    FORMAT(3H V=,F12.4,3H A=,F12.4,6H MACH=,F12.4)
      STOP
20    COEFF=1./SQRT(1.-MACH**2)
      CL=CLALPH*ALPHA*COEFF
      RETURN
      END


.TYPE DLO:ANGOFA.FOR
      FUNCTION ANGLE(Y,GAM,ANGIN,IA,GAMMAD)
      IF(IA .EQ. 1) GO TO 20
      IF(GAM .LE. GAMMAD*3.14159/180.) GO TO 20
      IA=0
      ANGLE=0.
      RETURN
20    ANGLE=ANGIN
      IA=1
      RETURN
      END
```

B. Wing Moment Formulation

From Figure 10 we have:

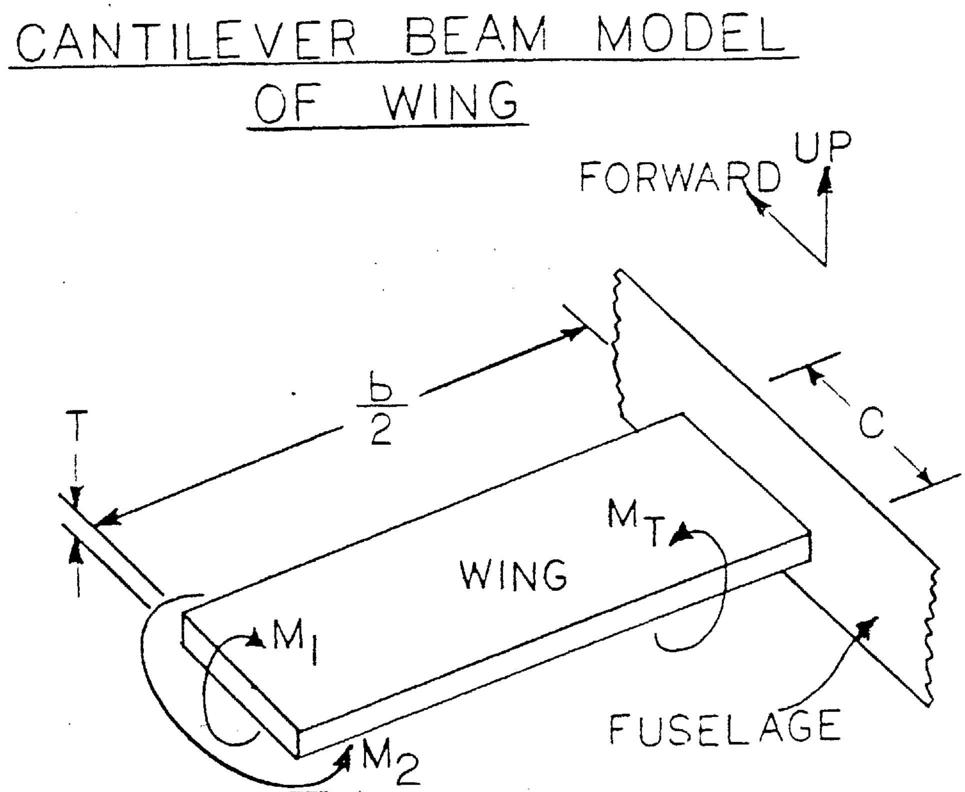

since $S = b \times c = \dfrac{W_g}{W_g/S}$ and $AR = b/c$

$$b = \sqrt{AR\,S} = \left[\frac{AR\,W_g}{W_g/S}\right]^{1/2} \tag{1}$$

The lift distribution is assumed to be constant along the wing (a consevative estimate) and is

$$w_1 = \frac{W_g}{b} = \frac{W_g}{\left[\frac{AR\ W_g}{W_g/S}\right]^{1/2}} \tag{2}$$

The maximum moment on a cantilever beam with a uniformly distributed load occurs at the root and is

$$M_{max} = \frac{q\,l^2}{2} \tag{3}$$

In this case $q = w_1 \times n_1 \times S.F._1$; $l = b/2$ so substituting these into (3) and combining with (1) and (2) gives

$$M_{1_{max}} = \frac{W_g^{3/2}\left[\frac{AR}{W_g/S}\right]^{1/2}}{8}\, n_1\, S.F._1 \tag{4}$$

The force distribution that creates M is the inertial loading from the mass of the wing under acceleration. This is given by

$$w_2 = \frac{W_w}{b} = \frac{W_w}{\left[\frac{AR\ W_g}{W_g/S}\right]^{1/2}} \tag{5}$$

Assuming that the wing is uniform. Then with

$q = w_2 \times n_2 \times S.F._2$ and $l = b/2$

$$M_{2_{max}} = \frac{W_w\left[\frac{AR\ W_g}{W_g/S}\right]^{1/2}}{8}\, n_2\, S.F._2 \tag{6}$$

C. Longitudinal Static Stability Determination

The derivation of the longitudinal static stability is taken from reference 6.

Horizontal Tail Lift

$$L_{T(\text{horiz. Tail})} = \frac{C_{m_0} \frac{1}{2} \rho_{air} V^2 S c + (h_1 - h_0) c L}{l_H} \tag{1}$$

Horizontal Tail Lift Coefficient

$$C_{L_T(\text{horiz. Tail})} = \frac{L_{T(\text{horiz. Tail})}}{\frac{1}{2} \rho_{air} V^2 S_H} \tag{2}$$

The tail incidence angle is given by

$$\alpha_T = \frac{C_{LT(h.T.)}}{a_1} - \frac{a_2}{a_1} \eta \tag{3}$$

Where η , the Elevator angle to trim, is given by

$$\eta = \frac{(1+F) C_{LT(h.T)} - \frac{a_1}{a}\left(1 - \frac{\partial \epsilon}{\partial \alpha}\right) C_L - a_1 \eta_T}{a_2} \tag{4}$$

F , a correction factor, is given by

$$F = \frac{a_1}{a} \frac{S_H}{S} \left(1 - \frac{\partial \epsilon}{\partial \alpha}\right) \tag{5}$$

The stick-fixed neutral point is given by

$$h_n = h_o + \frac{\bar{V}'}{1+F}\left(1 - \frac{\partial\epsilon}{\partial\alpha}\right) \qquad (6)$$

and

$$\bar{V}' = \frac{S_H}{S}\frac{l_H}{C} \qquad (7)$$

From this the Static Margin can be determined

$$K_n = (h_n - h_1) \qquad (8)$$

For the aircraft to be longitudinally statically stable, $K_n > 0$.

D. Dynamic Stability Derivative Formulation

The formulation for the dynamic stability derivatives is taken from reference 7, and has been modified to take into account that the glider has no engine.

1) Longitudinal Stability Derivatives

a - lift curve slope of the wing, given by

$$a = a_0\left(\frac{\pi A\!\!R}{a_0 + \pi A\!\!R}\right)$$

Where a_0 is the theoretical lift curve slope of a 2-dimensional wing, normally taken as $a \approx 2 \times \pi$.

C_{L_α} - lift curve slope of the aircraft as a whole

$$C_{L_\alpha} = \frac{\partial C_L}{\partial \alpha} = a\left\{1 + \frac{S_H}{S}\frac{a_1}{a}\left(1 - \frac{\partial \epsilon}{\partial \alpha}\right)\right\}$$

C_{m_α} - change in moment coefficient with angle of attack

$$C_{m_\alpha} = \frac{\partial C_m}{\partial \alpha} = a(h - h_n) = -a K_n$$

C_{X_α} - change in X-direction (drag) force with angle of attack

$$C_{X_\alpha} = \frac{\partial C_X}{\partial \alpha} = C_L\left(1 - \frac{2 C_{L_\alpha}}{\pi A\!\!R\, \epsilon_0}\right)$$

where ϵ_0 is a wing efficiency factor, here taken as 0.95

C_{z_α} - change in Z-direction force with angle of attack

$$C_{z_\alpha} = \frac{\partial C_z}{\partial \alpha} = -C_{L_\alpha} + C_{D_0}$$

C_{x_u} - change in the X-direction force with change in forward velocity and is, as such, the "speed damping" derivative.

$$C_{x_u} = \frac{\partial C_x}{\partial u} = -2\, C_{D_0}$$

C_{z_q} - change in lift due to the pitching velocity

$$C_{z_q} = \frac{\partial C_z}{\partial q} = -2\, a_1 V_H$$

C_{m_q} - change in moment coefficient with pitching velocity

$$C_{m_q} = \frac{\partial C_m}{\partial q} = C_{z_q} \frac{l_H}{c}$$

$C_{z_{\dot\alpha}}$ - change in Z-direction force with rate of angle of attack changes

$$C_{z_{\dot\alpha}} = \frac{\partial C_z}{\partial \dot\alpha} = C_{z_q} \frac{\partial \epsilon}{\partial \alpha}$$

$C_{m_{\dot\alpha}}$ - change in moment coefficient with rate of angle of attack changes

$$C_{m_{\dot\alpha}} = \frac{\partial C_m}{\partial \dot\alpha} = C_{z_{\dot\alpha}} \frac{l_H}{c}$$

2) Longitudinal Dimensional Parameters

l - characteristic length

$$l = c/2$$

μ - non-dimensional mass

$$\mu = \frac{Mg}{\rho_{air} S l}$$

t* - characteristic time

$$t^* = l/V$$

i_B - non-dimensional moment of inertia about the Y-axis (Pitch axis)

$$i_B = \frac{B}{\rho_{air} S l^3}$$

3) Lateral Stability Derivatives

C_{y_β} - change in sideforce due to sideslip angle

$$C_{y_\beta} = \frac{\partial C_y}{\partial \beta} = -C_{L_{\alpha(vertical\,tail)}} \frac{S_v}{S}$$

C_{l_β} - change in rolling moment due to sideslip angle

$$C_{l_\beta} = \frac{\partial C_l}{\partial \beta} = \left[1.2\sqrt{AR}\,\frac{z_w}{b^2}(h+w)\right] - \left[C_{L_{\alpha(v.t)}} \frac{S_v}{S}\frac{z_t}{b}\right] - \left[\frac{\partial C_{l_\beta}}{\partial C_L} C_L\right] - \left[\frac{\partial C_{l_\beta}}{\partial \Gamma} \Gamma\right]$$

This derivative is the dihedral effect, and is the major determinant of directional stability.

C_{n_β} - change in yawing moment due to sideslip angle, known as the weathercocking derivative.

$$C_{n_\beta} = \frac{\partial C_n}{\partial \beta} = \left[C_{L_\alpha (V.T.)} \frac{S_V}{S} \frac{l_V}{b}\right] - \left[1.3 \frac{h\,(\text{fuselage volume})}{W S b}\right] + \left[\frac{\partial C_{n_\beta}}{\partial C_L^2} C_L^2\right]$$

C_{y_β} - change in Y-direction force with roll rate, in these cases negligible

$$C_{y_\beta} = \frac{\partial C_y}{\partial \beta} \approx 0$$

C_{n_p} - change in yawing moment due to roll, and is the cause of the cross coupling of roll and yaw

$$C_{n_p} = \frac{\partial C_n}{\partial p} = \left[2\, C_{L_\alpha (V.T.)} \frac{S_V}{S} \frac{l_V}{b} \frac{Z_f}{b}\right] - \left[\frac{\partial C_{n_p}}{\partial C_L} C_L\right]$$

C_{l_p} - change in rolling moment with roll, and is known as the roll-damping derivative. It is obtained from reference 7, pg. 487 .

$$C_{l_p} = \frac{\partial C_l}{\partial p} = -\ \text{constant}$$

C_{y_r} - change in Y-direction force with yaw rate

$$C_{y_r} = \frac{\partial C_y}{\partial r} = 2\, C_{L_\alpha (V.T.)} \frac{S_V}{S} \frac{l_V}{b}$$

C_{l_r} - change in rolling moment due to yaw rate, and is another cause of yaw-roll cross-coupling.

$$C_{l_r} = \frac{\partial C_l}{\partial r} = \left[C_{y_r} \frac{Z_f}{b}\right] + \left[\frac{\partial C_{l_r}}{\partial C_L} C_L\right]$$

C_{n_r} - change in yawing moment due to yaw rate, and is the yaw damping derivative

$$C_{n_r} = \frac{\partial C_n}{\partial r} = \left[-C_{y_r} \frac{l_V}{b}\right] - \left[\frac{\partial C_{n_r}}{\partial C_L^2} C_L^2\right] - \left[0.3\, C_{D_0}\right]$$

4) Lateral Dimensional Parameters

l - characteristic length

$$l = b/2$$

μ - non-dimensional mass

$$\mu = \frac{Mg}{\rho_{air} S l}$$

t^* - characteristic time

$$t^* = l/V$$

i_A - non-dimensional moment of inertia about the X-axis (roll axis).

$$i_A = \frac{A}{\rho_{air} S l^3}$$

i_C - non-dimensional moment of inertia about the Z-axis (yaw axis).

$$i_C = \frac{C}{\rho_{air} S l^3}$$

i_E - non dimensional product of inertia about the Y-axis (pitch axis).

$$i_E = \frac{E}{\rho_{air} S l^3}$$

E) Dynamic Stability Determination

1) Longitudinal Dynamic Stability (Stick Fixed)

a) Exact Solutions:

The equations of motion used here were developed in reference 7, as was the characteristic matrix resulting from the equation of motion.

The characteristic matrix for longitudinal motion is:

$$\begin{vmatrix} (2\mu\lambda - C_{x_u}) & -C_{x_q} & C_L \\ (2C_L - C_{z_u}) & (2\mu\lambda - C_{z_{\dot\alpha}}\lambda - C_{z_\alpha}) & -\lambda(2\mu + C_{z_q}) \\ -C_{m_u} & -(C_{m_{\dot\alpha}}\lambda + C_{m_\alpha}) & (i_B\lambda^2 - C_{m_q}\lambda) \end{vmatrix} = 0$$

This is the stability determinant and gives a fourth order characteristic equation of the dynamic system. Expansion of this leads to

$$A\lambda^4 + B\lambda^3 + C\lambda^2 + D\lambda + E = 0$$

where $$A = 2\mu i_B (2\mu - C_{z_{\dot\alpha}})$$

$$B = -2\mu i_B (C_{z_\alpha} + C_{x_u}) + i_B C_{x_u} C_{z_{\dot\alpha}} - 2\mu(C_{z_q} C_{m_{\dot\alpha}} - C_{m_q} C_{z_{\dot\alpha}}) - 4\mu^2 (C_{m_{\dot\alpha}} + C_{m_q})$$

$$C = i_B (C_{x_u} C_{z_\alpha} - C_{x_\alpha} C_{z_u}) + 2\mu(C_{z_\alpha} C_{m_q} - C_{m_\alpha} C_{z_q} + C_{x_u} C_{m_q} + C_{m_{\dot\alpha}} C_{x_u}) - (4\mu^2 C_{m_\alpha}) - C_{x_u}(C_{m_q} C_{z_{\dot\alpha}} - C_{z_q} C_{m_{\dot\alpha}}) + 2 C_L C_{x_\alpha} i_B$$

$$D = -2 C_L^2 C_{m_{\dot\alpha}} + 2\mu(C_{x_u} C_{m_\alpha} - C_{x_\alpha} C_{m_u} + C_L C_{m_u}) + C_{x_u}(C_{m_\alpha} C_{z_q} - C_{m_q} C_{z_\alpha}) - C_{x_\alpha}(C_{m_u} C_{z_q} - C_{m_q} C_{z_u}) - C_L(C_{m_u} C_{z_{\dot\alpha}} - C_{z_u} C_{m_{\dot\alpha}}) - 2 C_L C_{m_q} C_{x_\alpha}$$

$$E = -C_L\left[C_{m_\alpha}(2C_L - C_{z_u}) + C_{m_u} C_{z_\alpha}\right]$$

Solving the characteristic equation for λ gives two pairs of complex conjugate roots

$$\lambda_{1,2} = -\zeta_1 \omega_{n_1} \pm i\,\omega_{n_1}\sqrt{1-\zeta_1^2} \quad ; \quad \lambda_{3,4} = -\zeta_2 \omega_{n_2} \pm i\,\omega_{n_2}\sqrt{1-\zeta_2^2}$$

The first set of roots, $\lambda_{1,2}$, is a long period, lightly damped mode and is called the phugoid mode.

The second set of roots, $\lambda_{3,4}$, is a short period, much more heavily damped oscillation, and is known as the short period mode.

B) Approximate Solutions:

Approximate solutions for the phugoid and the short period mode are given by the following equations:

i) Phugoid Mode:

$$\lambda_{1,2} = -\zeta_1 \omega_{n_1} \pm i\,\omega_{n_1}\sqrt{1-\zeta_1^2}$$

where

$$\omega_{n_1} = \frac{C_L}{\sqrt{2}\,\mu} \qquad \zeta_1 = \frac{C_{X_u}}{2\sqrt{2}\,C_L}$$

The approximate values for the phugoid mode are accurate to within 20% of the exact values.

ii) Short Period Mode:

$$\lambda_{3,4} = -\zeta_2 \omega_{n_2} \pm i\,\omega_{n_2}\sqrt{1-\zeta_2^2}$$

where

$$\omega_{n_2} = \left[\frac{C_{Z_\alpha} C_{m_q} - 2\mu C_{m_\alpha}}{2\mu i_B}\right]^{1/2}$$

$$\zeta_2 = -\frac{2\mu C_{m_q} + i_B C_{Z_\alpha} + 2\mu C_{m_{\dot{\alpha}}}}{2\left[2\mu i_B\left(C_{Z_\alpha} C_{m_q} - 2\mu C_{m_\alpha}\right)\right]^{1/2}}$$

The approximate values for the short period mode are the same as the exact values to within the accuracy of the calculation.

For both the phugoid and short period modes the period of oscillations, amplitude halving time, and cycles to halve are the important parameters. These are given by:

$$\text{PERIOD} : \quad T = \frac{2\pi}{\omega_n \sqrt{1-\zeta^2}} t^*$$

$$\text{HALVING TIME} : \quad t_{half} = \frac{0.69}{\zeta \omega_n} t^*$$

$$\text{CYCLES TO HALVE} : \quad N_{half} = \frac{t_{half}}{T}$$

2) Lateral Dynamic Stability (Stick Fixed)

Again, the equations of motion and resulting characteristic matrix used here were developed in reference 7.

The characteristic matrix for lateral motion is:

$$\begin{vmatrix} (2\mu\lambda - C_{y_\beta}) & -(C_{y_p}\lambda + C_L) & (2\mu - C_{y_r}) \\ -C_{\ell_\beta} & (i_A\lambda^2 - C_{\ell_p}\lambda) & -(i_E\lambda + C_{\ell_r}) \\ -C_{n_\beta} & -(i_E\lambda^2 + C_{n_p}\lambda) & (i_C\lambda - C_{n_r}) \end{vmatrix} = 0$$

This stability determinant gives a fourth order characteristic equation of the dynamic system. Expansion leads to:

$$A\lambda^4 + B\lambda^3 + C\lambda^2 + D\lambda + E = 0$$

where

$$A = 2\mu\left(i_A i_C - i_E^2\right)$$

$$B = C_{y_\beta}\left(i_E^2 - i_A i_C\right) - 2\mu\left[i_C C_{l_p} + i_A C_{n_r} + i_E\left(C_{l_r} + C_{n_p}\right)\right]$$

$$C = 2\mu\left[C_{n_r} C_{l_p} - C_{n_p} C_{l_r} + i_A C_{n_\beta} + i_E C_{l_\beta}\right] + i_A\left(C_{y_\beta} C_{n_r} - C_{n_\beta} C_{y_r}\right)$$
$$+ i_C\left(C_{y_\beta} C_{l_p} - C_{l_\beta} C_{y_p}\right) + i_E\left(C_{y_\beta} C_{n_p} - C_{n_\beta} C_{y_p} + C_{l_r} C_{y_\beta} - C_{l_\beta} C_{y_r}\right)$$

$$D = C_{y_\beta}\left(C_{l_r} C_{n_\beta} - C_{n_r} C_{l_\beta}\right) + C_{y_p}\left(C_{l_\beta} C_{n_r} - C_{n_\beta} C_{l_r}\right)$$
$$+ \left(2\mu - C_{y_r}\right)\left(C_{l_\beta} C_{n_p} - C_{n_\beta} C_{l_p}\right) - C_L\left(i_C C_{l_\beta} + i_E C_{n_\beta}\right)$$

$$E = C_L\left[C_{l_\beta} C_{n_r} - C_{n_\beta} C_{l_r}\right]$$

Solving the characteristic equation [either by computer program (ACCESS) or long division] gives two real roots plus one pair of complex conjugate roots.

$$\lambda_1 \,, \quad \lambda_2 \,, \quad \lambda_{3,4} = -\zeta_3 \omega_{n_3} \pm i\,\omega_{n_3}\sqrt{1 - \zeta_3^2}$$

The first root, λ_1 , is the smaller real root and defines the spiral mode. It has a steady decay, with a halving time given by:

$$t_{half} = \frac{0.69}{\lambda_1} t^*$$

The second root, , the larger of the real roots, defines the rolling mode. It also has a steady decay, with a halving time given by:

$$t_{half} = \frac{0.69}{\lambda_2} t^*$$

The complex conjugate pair defines the lateral oscillations, also known as dutch roll. It has a period, halving time, and cycles to halve given by:

PERIOD : $T = \dfrac{2\pi}{\omega_{n_3}\sqrt{1-\zeta_3^2}} t^*$

HALVING TIME : $t_{half} = \dfrac{0.69}{\omega_{n_3}\zeta_3} t^*$

CYCLES TO HALVE : $N_{half} = \dfrac{t_{half}}{T}$

X. BIOGRAPHICAL NOTE

The author was born during August, 1957 in northern Manhattan, and lived there till the age of six. Along with his parents and sibling(s) he moved to Englewood, New Jersey for the remainder of his formative years, attending Dwight Morrow High School in the process. He left the comforts of upper middle class suburban life in September 1975 to attend the Massachusetts Institute of Technology in Cambridge, Massachusetts, with the intent to study Physics and/or Mathematics. Coming to his senses late in his sophomore year, he majored in Aeronautical Engineering, while also taking many courses in the Mechanical Engineering Department. He was graduated in December 1979 with a 4.55/5.0 G.P.A., having once won the "Wunsch Silent Crane and Hoist" award for outstanding design of an Algal Harvester, for design work accomplished in a Mechanical Engineering design course.

For three summers the author worked at "Kovar Engineering Services", a precision machine shop, and became proficient on the miller, lathe, surface grinder, and many other machine tools. He enjoyed working with his hands and felt it indispensible for an engineer to know and understand machine shop practices.

Mr. Zeitlin began attending graduate school at M.I.T. in the Aeronautiical Engineering Department in February 1980 and promptly won another "Wunsch Silent Crane and Hoist" award for outstanding desing of a Glare Screen Mount, for work accomplished in an advanced Mechanical Engineering design course.

After he is graduated (again) in August 1981, Mr. Zeitlin plans to live and work in the Boston area.

XI. BIBLIOGRAPHY

1) Welch, Ann Lorne, and Irving, Frank. New Soaring Pilot. 2nd ed. London: John Murray, 1970.

2) Abbott, Ira H., and von Doenhoff, Albert. Theory of Wing Sections. New York: McGraw Hill, 1949.

3) Althaus, D. Stuttgarter Profilkatalog. Stuttgart: Instituts for Aerodynamik and Gasdynamik, 1972.

4) Perkins, Courtland D., and Hage, Robert E. Aircraft Performance, Stability, and Control. New York: Wiley, 1949.

5) Dwinnell, James H. Principles of Aerodynamics. New York: McGraw Hill, 1949.

6) Irving, Francis G. An Introduction to the Longitudinal Static Stability of Low Speed Aircraft. Oxford, New York: Pergamon Press, 1966.

7) Etkin, Bernard. Dynamics of Flight: Stability and Control. New York: Wiley, 1959.

8) Rivello, Robert M. *Theory and Analysis of Flight Structures.* New York: McGraw Hill, 1969.

9) Peery, David J. *Aircraft Structures.* New York: McGraw Hill, 1950.

10) Hanson, P.W., ed. *Science and Technology of Low Speed and Motorless Flight.* Washington: NASA, 1979.

11) Marsden, D. J. "Sailplane Performance Estimation". *Technical Soaring,* Volume V, number 3.

12) Larrabee, E.E. "The Aerodynamic Design of Sailplane Tail Assemblies." *Technical Soaring,* Volume V, number 1.

13) Squires, P.K. "Configuration Optimization of a 13-meter Span Sport Sailplane." *Technical Soaring,* Volume IV, number 3.

14) Goodhart, H.C.N. "A Note on the Measurement of the Induced Drag Factor (k) of a Glider." *Technical Soaring,* Volume I, number 4.

15) Glade, T.W., and Westkaemper, J.C. "Planform Effects on the Induced Drag of Untwisted Wings." *Technical Soaring,* Volume I, number 2.

16) Wortmann, F.X. "Drag Reduction in Sailplanes." Soaring, June-July 1966.

17) Jones, R.T. "Minimizing Induced Drag." Soaring, October 1979.

18) McMasters, John H., and Nash-Webber, James L. "Some Technical Extrapolations." Soaring, January, 1977.

19) Sato, Hiroshi. "Spanwise Distribution of aerodynamic Shear and Bending Moment on Cantilever Tapered Wings." 10th O.S.T.I.V. Congress Publication, June 1975.

20) Nash-Webber, James L. "The Effect of Wing Loading on the Performance of Advanced Sailplanes." S.S.A. - A.I.A.A. Symposium. March 1974.

21) Nash-Webber, James L., ed. NASA CR-2315, Washington: NASA, November 1973.

22) Abold, Phillip L. "Design of a Deployable Wing Glider." M.S. Thesis, Air Force Institute of Technology, December 1974.

23) Snapp, Elbridge Lee III. "A Preliminary Design of a Remotely Controlled Glider for Long-Line Operation."

M.S. Thesis, Air Force Institute of Technology, June 1973.

24) Mar, J.W. "Research on the Exploitation of Advanced Composite Materials to Lightly Loaded Structures." Washington: NASA, November 1973.

25) Zeitlin, Marc J. "16.29 Class Notes (Design With Filamentary Composite Materials)." Cambridge, May 1980.

26) Paluszek, Michael A. "Trajectory Analysis for an Electromagnetically Launched Glider." Cambridge, April 1980.